Acta Biochim Biophys Sin 2025, 57(x): 1–17
https://cstr.cn/32197.14.abbs.2025075
https://doi.org/10.3724/abbs.2025075
Original Article

Original Article

FGF8 promotes lipid droplet accumulation via the FGFR1/p-p38 axis in chondrocytes

Minglei Huang[1], Haoran Chen[1], Jieya Wei[1], Caixia Pi[1], Mengmeng Duan[1], Xiaohua Pu[1], Zhixing Niu[1], Siqun Xu[1], Shasha Tu[1], Sijun Liu[1], Jiazhou Li[1], Li Zhang[1], Yang Liu[1], Hao Chen[1], Chunming Xu[2], and Jing Xie[1,*]

[1]State Key Laboratory of Oral Diseases & National Center for Stomatology & National Clinical Research Center for Oral Diseases, West China Hospital of Stomatology, Sichuan University, Chengdu 610041, China, and [2]School of Basic Medicine, Gannan Medical University, Ganzhou 341000, China
*Correspondence address. Tel: +86-28-85503469; E-mail: xiejing2012@scu.edu.cn

Received 18 February 2025 Accepted 15 April 2025 Published 15 May 2025

Abstract
Chondrocytes store lipids in the form of lipid droplets (LDs) and maintain cartilage lipid metabolic homeostasis by consuming or regenerating LDs. This modulation is largely mediated by a series of biochemical factors. Fibroblast growth factor 8 (FGF8) is one of the most important factors involved in the proliferation, differentiation, and migration of chondrocytes and has attracted increasing attention in the physiology and pathology of cartilage. However, the effect of FGF8 on LD accumulation in chondrocytes remains unclear. This study aims to elucidate the role of FGF8 in LDs and explore the underlying biomechanism involved. The results reveal that FGF8 promotes LD accumulation in chondrocytes by upregulating perilipin1 (Plin1) expression. FGF8 activates the cytoplasmic p-p38 signaling pathway via fibroblast growth factor receptor 1 (FGFR1) to increase LD accumulation in chondrocytes. Subsequent experiments with siRNAs and specific inhibitors further confirm the importance of the FGFR1/p38 axis for LD accumulation in chondrocytes exposed to FGF8. The results increase our understanding of the role of FGF8 in the lipid metabolic homeostasis of chondrocytes and provide insights into the physiology and pathology of cartilage.

Key words FGF8, lipid droplet, chondrocyte, Plin1, FGFR1, p-p38

Introduction

The lipid droplet (LD), a principal hub organelle for intracellular lipid storage, consists of a neutral lipid core enveloped by a phospholipid monolayer membrane [1–3]. LD biogenesis begins mostly in the endoplasmic reticulum (ER), the main organelle involved in neutral lipid synthesis [4]. The first step in LD biosynthesis is the synthesis of neutral lipids such as triacylglycerols (TGs) and cholesterol esters (CEs) in the ER [4,5]. These neutral lipids are dispersed in the ER at low concentrations. With continuous neutral lipid synthesis, biophysical processes result in the formation of a neutral lipid lens (also called the oil lens) [5]. A widely recognized model states that neutral lipids nucleate an oil phase that minimizes the entropy costs involved in disrupting the ER bilayer membrane [1,4,5]. Subsequently, the oil phase transitions to the oil lens. The oil lens accommodates more neutral lipids and promotes the aggregation of neutral lipids to form LDs [5]. After being released into the cytoplasm, these nascent LDs gradually develop into larger mature LDs by storing more lipids or merging with each other [3–5]. In addition, LDs interact with other organelles, such as mitochondria and lysosomes, to regulate their metabolism and function. For example, Meng *et al.* [6] reported that phosphofructokinase, a glycolytic enzyme, promotes LD-mitochondrion tethering to increase β-oxidation. Menon *et al.* [7] reported that ARL8B, a GTPase, promotes LD-lysosome contact and induces lysosomal lipolysis of LDs. More importantly, lipophagy, an autophagy process that specifically targets LDs, plays an important role in maintaining the cellular energy supply and alleviating metabolic diseases such as atherosclerosis [8]. Lin *et al.* [9] reported that the recovery of lipophagy via the inhibition of PPAR/PI3K/AKT signaling relieves atherosclerosis-related symptoms, including lipid

accumulation, apoptosis, and inflammation.

The primary function of intracellular LDs is to serve as storage reservoirs for neutral lipids and supply essential lipid precursors whenever the cellular lipid level decreases [10]. These neutral lipids can be used for cell energy supply through mitochondrial β-oxidation and for structural composition, such as lipid membrane expansion [10]. In addition, LDs can assist cells in preventing lipid toxicity [11]. Free lipids such as fatty acids can act as detergents to disrupt the cell membrane structure. Synthesizing fatty acids into triglycerides and storing them in LDs effectively prevents intracellular lipid toxicity. However, despite the numerous positive effects of LDs within cells, excessive LD accumulation can result in the development of various diseases, such as hepatic steatosis [10,11]. As organelles with important functions in cells, LDs are also regulated by a variety of proteins [12]. These proteins, including a series of enzymes that regulate the dynamic process of LD biogenesis and linker proteins that connect LDs to other organelles, regulate LD activities [12]. These proteins are roughly divided into two types: integral and peripheral proteins. Integral proteins are inserted into the monolayer membrane of LDs and can recruit peripheral proteins to LDs [12]. Integral proteins play vital roles in the generation, maintenance, and lipolysis of LDs and are composed of two functional subclasses according to their trafficking pathways. One is a Class I LD protein that originates in the ER [12]. These proteins are then transferred to LDs during LD formation. For example, seipin, a typical ER protein located at the site of LD budding, can form a flexible cage to promote LD formation [13]. Furthermore, it plays a pivotal role in facilitating the connection between nascent LDs and the ER and enhancing the transfer of lipids and proteins from the ER to LDs [14]. In addition to seipin, some lipid synthase- and ubiquitination-related proteins, such as diacylglycerol acyltransferase 2 (DGAT2) and ancient ubiquitous protein 1 (AUP1) [15–17], also belong to this subclass. Malis *et al.* [17] reported that DGAT2 is transferred from the ER to the LD surface and promotes LD growth. Smith *et al.* [18] reported that AUP1 can reduce the formation of misfolded proteins and is thus important for protein quality control in the progression of LD formation and maturation. Moreover, a decrease in AUP1 expression can reduce the accumulation of cellular lipids and affect the final formation of LDs [15,16,19]. The other is the Class II LD protein, which is synthesized in the cytoplasmic ribosome and targets LDs. The typical protein is the perilipin (Plin) protein family which contains five family members (Plin1-5) [12,20]. The main function of Plins is to inhibit the lipolysis of LDs, but in the case of an urgent need for a large number of liposomes, Plins can be phosphorylated with the help of protein kinase A (PKA), and the phosphorylated Plins then recruit lipases such as adipose triglyceride lipase (ATGL) and hormone-sensitive lipase (HSL) to achieve lipolysis. In addition, Plins play a role in the interactions between LDs and other organelles. For example, Miner *et al.* [21] reported that phosphorylated Plin5 interacts with fatty acid transport protein 4 (FATP4) to promote the interaction between LDs and mitochondria, which facilitates fatty acid transport from LDs to mitochondria.

Cartilage tissue is characterized by the absence of blood vessels, lymphatic vessels, and nerves [22,23]. Owing to its unique composition, which is composed mainly of type II collagen and proteoglycans, cartilage tissue has superior performance in the resistance to compression and decompression but also has extremely poor healing ability once injury or damage occurs [24,25]. Cartilage injury or damage can lead to osteoarthritis (OA), a typical degenerative disease [26]. Recent studies have revealed that OA pathogenesis is highly similar to that of systemic metabolic syndrome (MS), with lipid metabolism disorder as a vital indicator [27–29]. For example, Park *et al.* [30] reported that excessive LD accumulation in chondrocytes induced by PPARα or ACOT12 deficiency accelerated the degradation of the cartilage matrix in OA and suggested that a reduction in LD accumulation in chondrocytes may be a potential therapeutic target for OA. Wang *et al.* [31] reported that GDF11 inhibits abnormal lipid formation and LD accumulation by promoting the ubiquitination of PPARγ in chondrocytes in temporomandibular joint osteoarthritis (TMJOA). Chondrocytes can obtain nutrients only from the subchondral bone and the surrounding synovial fluid, indicating that chondrocytes need to store sufficient raw lipid materials as energy reserves [32,33]. These raw lipids stored in cellular LDs include fatty acids, triacylglycerols, cholesterol esters, and their byproducts, including prostaglandins and leukotrienes [34]. Healthy chondrocytes have high levels of omega-9 fatty acids (n-9 FAs) and low levels of omega-6 polyunsaturated fatty acids (n-6 PUFAs) [35]. With increasing chondrocyte age, the content of n-6 PUFAs increases, whereas that of n-9 FAs decreases. In addition, arachidonic acid (a typical inflammation-related lipid) and n-6 PUFAs are also increased in osteoarthritic chondrocytes compared with healthy chondrocytes [36]. After binding to glycerol, triacylglycerol is the main intracellular storage form of fatty acids. When chondrocytes urgently require fatty acids, triacylglycerols are gradually broken down into fatty acids and glycerol by a variety of catabolic enzymes to provide the raw material supply for mitochondrial aerobic respiration [1,35]. Cholesterol esters also affect the growth, physiological activity, and differentiation of chondrocytes [35]. When the regulatory proteins that assist in the transport of cholesterol esters out of chondrocytes are inhibited, cholesterol esters accumulate in chondrocytes, leading to sharp deterioration of the OA cartilage matrix [37]. In addition, prostaglandins and leukotrienes have been recognized for their roles in promoting inflammatory responses in cartilage joints, although their proportion of lipids is much lower. Both prostaglandins and leukotrienes are biosynthesized from arachidonic acid via prostaglandin synthase and lipoxygenase, respectively [38,39]. Prostaglandin E2 (PGE2), a typical prostaglandin, has been implicated in promoting chondrocyte hypertrophy. Interestingly, a recent study revealed an unexpected role for PGE2, showing that it inhibited the production of related hypertrophy signals in hypertrophic chondrocytes [40]. Leukotriene B4 (LTB4), a potent proinflammatory leukotriene synthesized by leukotriene A_4 hydrolase (LTA_4H), has been shown to be associated with cartilage matrix degeneration [41].

LD formation and maturation are mediated by a series of biochemical factors, including interleukins, heparan sulfates, and transforming growth factors, during OA progression [42,43]. FGF8, an important member of the fibroblast growth factor family, plays a vital role in chondrocyte proliferation, differentiation, and extracellular matrix synthesis during the early stages of vertebrate development [44,45]. In cartilage diseases, FGF8 has been implicated in the pathogenesis of Kashin-Beck disease, where it disrupts chondrogenic differentiation through FGFR3 and enhances chondrocyte proliferation and hypertrophy [46]. FGF8 has been reported to promote cartilage degradation and exacerbate OA by increasing the production of matrix metalloproteinase-3 [37,44,47].

We recently confirmed that FGF8 regulates the expression of gelatinases (Mmp-2 & -9) and thus has a direct effect on the degradation of the cartilage matrix [48]. However, whether and how FGF8 participates in lipid metabolism in chondrocytes during OA progression remain unclear.

In this study, we aimed to investigate the role of FGF8 in the accumulation of LDs in chondrocytes and to explore the underlying biomechanisms involved. tOur results increase the understanding of lipid accumulation in chondrocytes and provide potential strategies for the prevention and treatment of osteoarticular diseases.

Materials and Methods

Chondrocyte acquisition and culture

All experiments involving animal samples (mouse samples) were conducted in accordance with the protocols and ethical principles approved by the Institutional Review Board at the West China Hospital of Stomatology (No. WCHSIRB-CT-2022–127). Primary chondrocytes were obtained as previously described [49,50]. First, articular cartilage was isolated from newborn C57BL/6J mice (2–3 days old) and immersed in phosphate-buffered saline (PBS) supplemented with 1% penicillin-streptomycin (SV30010; HyClone, Logan, USA). The articular cartilage was subsequently digested with 0.25% trypsin (25200056; Thermo Fisher Scientific, Waltham, USA) for 30 min at 37°C and then treated with 0.5% type II collagenase (C6885; Sigma, St Louis, USA) in Dulbecco's modified Eagle's medium (DMEM; SH30243.01B; HyClone) for 12 h at 37°C. Next, the digested solution was neutralized with DMEM supplemented with 10% fetal bovine serum (FBS; SH30406.06; HyClone) and centrifuged at 172 *g* for 8 min. The supernatant was discarded, and the chondrocytes in the pellet were resuspended in fresh DMEM containing 1% penicillin-streptomycin and 10% FBS. Chondrocytes were then incubated at 37°C in a humidified atmosphere with 5% CO_2, and the culture medium was changed every two days. The first three generations of chondrocytes were used for subsequent experiments.

Transfection of small interfering RNA (siRNA)

Chondrocytes were cultured in antibiotic-free 10% FBS DMEM for 24 h and then transfected with 50 nM siRNA according to the manufacturer's instructions. The transfection reagent used in this study was Lipofectamine RNAiMAX (13778075; Invitrogen, Burlington, Canada). Chondrocytes transfected with si-NC were used as negative controls. The siRNAs were obtained from Hanbio (Shanghai, China) with the sequences as follows: si-NC: sense, 5′-UUCUCCGAACGUGUCACGUTT-3′, anti-sense, 5′-ACGUGACACG UUCGGAGAATT-3′; si-Plin1: sense, 5′-GGCUCUGUCAUCAUCU AUATT-3′, anti-sense, 5′-UAUAGAUGAUGACAGAGCCTT-3′; and si-FGFR1: sense, 5′-AGAUCCCGGCUCUUCAAUATT-3′, anti-sense, 5′-UAUUGAAGAGCCGGGAUCUTT-3′. The knockdown efficiency was verified by qPCR.

RNA extraction and quantitative real-time polymerase chain reaction (qPCR)

Chondrocytes were treated with FGF8 at 25 ng/mL for 12 h before RNA extraction. Total RNA was extracted using an RNA isolation kit (RE-03011; FOREGENE, Chengdu, China). After collection, the total RNA was reversely transcribed into complementary DNA (cDNA) using a reverse transcription kit (K1621, RevertAid; MBI, Panneviz, Lithuania). qPCR was performed using the SYBR Premix Ex II Taq PCR kit (RR820A; Takara, Tokyo, Japan) in a real-time PCR detection system (CFX 96; Bio-Rad, Hercules, USA). The sequences of primers used in this study included *β-actin* (forward: 5′-GGCTGTATTCCCCTCCATCG-3′, reverse: 5′-CCAGTTGGTAAC AATGCCATGT-3′), *FGFR1* (forward: 5′-GCTTCATCTACGG AATGTCTCC-3′, reverse: 5′-TCTTCCAGGGCGATAGAGTTAC-3′), and *Plin1* (forward: 5′-GACTGAGGTGGCGGTCTGCTGC-3′, reverse: 5′-GGGGTGGGCTTCTTTGGTGCTG-3′). The $2^{-\Delta\Delta Ct}$ method was used to analyze the results. *β-Actin* was used as an internal control.

RNA sequencing and STRING analysis

Total RNA was extracted from chondrocytes treated with FGF8 at 25 ng/mL for 24 h using Trizol (15596-018; Thermo Fisher Scientific) and sent to Shanghai Lifegenes (Shanghai, China) for transcriptome sequencing analysis as described in previous articles [51]. RNA integrity was assessed using the RNA Nano 6000 Assay Kit of the Bioanalyzer 2100 system (Agilent, Santa Clara, USA). The RNA input was set to 1.5 μg per sample. Index-coded samples were categorized using the HiSeq 4000 PE Cluster Kit (Illumina, San Diego, USA) according to the manufacturer's instructions. The read numbers of the genes were calculated using HTSeq v0.6.1, followed by fragments per kilobase of exon model per million mapped fragments (FPKM) calculation. A Pheatmap was generated using the R programming language. GO terms with a *P* value less than 0.05 were considered significantly enriched by differentially expressed genes (DEGs). Kyoto Encyclopedia of Genes and Genomes (KEGG) functional enrichment analysis was performed using KOBAS v3.0 software. Furthermore, we conducted STRING protein relationship analyses based on this data. By navigating to the *string-db.org* website and importing the sequencing outcomes, we successfully constructed a protein-protein interaction network, which provided valuable insights into the complex relationships among these proteins. The data obtained through RNA sequencing are shown in Supplementary Tables S1 and S2.

Western blot analysis

Western blot analysis was performed as previously described [52]. Chondrocytes were cultured in DMEM containing 10% FBS until they reached an appropriate density (80%–90% confluency). The culture medium was then replaced by DMEM containing 2% FBS to starve the chondrocytes for 12 h. Next, the chondrocytes were treated with FGF8 (100-25A; Peprotech, Rocky Hill, USA) at 5, 10, or 25 ng/mL in the presence or absence of SB203580 (HY-10256; MCE, Monmouth Junction, USA) at 20 μM in 1% FBS DMEM. At the indicated time points, the culture medium was discarded, and the chondrocytes were lysed using RIPA lysis buffer (P0013B; Beyotime, Shanghai, China) containing 1% PMSF (P7626; Sigma) in an ice bath. The lysates were mixed with an equal volume of loading buffer (1610737EDU; Bio-Rad) and boiled at 100°C for 5–10 min to prepare protein samples. The protein samples were separated by electrophoresis using 10% sodium dodecyl sulfate-polyacrylamide gels (1.0 mm) and transferred to PVDF membranes (IPVH00010; Millipore, Billerica, USA). The PVDF membranes were blocked with 5% skim milk for 1–2 h and incubated with primary antibodies overnight at 4°C. The primary antibodies used in this study were as follows: β-actin (200068-8F10, 1:1000, anti-mouse; Zenbio, Chengdu, China), Erk (343830, 1:1000, anti-rabbit; Zenbio), JNK (R22866, 1:1000, anti-rabbit; Zenbio), p38 (R25239,

1:1000, anti-rabbit; Zenbio), p-p38 (310091, 1:1000, anti-rabbit; Zenbio), p-Erk (310065, 1:1000, anti-rabbit; Zenbio), p-JNK (381100, 1:1000, anti-rabbit; Zenbio), and β-catenin (201328-5D6, 1:1000, anti-mouse; Zenbio). The PVDF membranes were then washed three times for 5 min each with Tris-buffered saline containing 0.05% Tween 20 (TBST). Next, the PVDF membranes were incubated with the corresponding secondary antibodies (511203 and 511103, 1:5000; Zenbio) for 2–3 h. Finally, signals on the PVDF membranes were detected via the Immobilon® Western Kit (P90719; Millipore). The signal results were analyzed using ImageJ software.

Immunofluorescence staining and BODIPY493/503 staining assay

The detailed immunofluorescent procedure was followed as previously described [53]. Briefly, the chondrocytes were washed three times with 1× PBS, fixed with 4% paraformaldehyde for 15 min, and permeabilized with 0.25% Triton X-100 (P0096; Beyotime) for 10 min. After permeabilization, the chondrocytes were blocked with 5% BSA (V900933; Sigma) for 2 h and incubated with primary antibodies including anti-Plin1 (3467, 1:200; CST, Danvers, USA) and anti-p-p38 (310091, 1:200; Zenbio) overnight at 4°C. After primary antibody incubation, the samples were incubated with the corresponding secondary antibody (Alexa Fluor 647 donkey anti-rabbit IgG; ab150075, 1:200; Abcam, Cambridge, UK) for 2 h. For LD staining, the chondrocytes were incubated with BODIPY493/503 dye (D3922; Thermo Fisher Scientific) for 10 min. Next, the chondrocyte cytoskeleton was stained with FITC (A12379; Invitrogen) at 4°C overnight. The chondrocyte nuclei were then stained with DAPI (D9542; Sigma) for 10 min. Immunofluorescence images were captured via a confocal laser scanning microscope (CLSM, FV3000; Olympus, Tokyo, Japan) and analyzed by ImageJ.

AAV-FGF8 animal model and immunofluorescence staining

FGF8 overexpression in articular cartilage was achieved by injecting an adeno-associated virus (AAV) carrying the *FGF8* gene, as previously described [50]. AAV-FGF8 was obtained from GENECHEM (Shanghai, China). The carrier used was CMV bGlobin-MCS-EGFP-3FLAG-WPRE-hGH polyA. The gene ID was 14179, and the transcript ID was NM_010205 in NCBI. Briefly, after the vector was digested with enzymes, the PCR-amplified target fragment is ligated to the vector. The ligated vector was subsequently transfected into DH5α sensory cells. After transfection, the DH5α sensory cells were cultured for 12–16 h, and the positive clones were screened for PCR identification. After PCR identification, the positive DH5α sensory cells were subjected to expansion culture and plasmid extraction. After the plasmid carrying *FGF8* was constructed, the constructed vector plasmid was transfected into 293T cells (cells packaged with AAV, adherent-dependent epithelial cells) via a triple plasmid transfection system (pAAV-RC plasmid, pHelper plasmid, or shuttle plasmid). After transfection with the plasmid carrying *FGF8*, the cell precipitates were collected for 72 h for virus purification. AAV-FGF8 was administered into the temporomandibular joint cavity under anesthetic conditions (5×10^{10} V.g/mL, 3 μL per joint). Temporomandibular cartilage samples were harvested after 4 weeks of injection. Immunofluorescence analysis was performed using antibodies or a liquid kit (BODIPY 493/503; Sgima). Briefly, the tissue samples were incubated with primary antibodies including anti-osterix (1:200, ab209484; Abcam) and anti-Plin1 (1:200, 3467; CST) overnight at 4°C. After incubation with the primary antibodies, the corresponding secondary antibodies (Alexa Fluor 647 donkey anti-rabbit IgG, 1:200, ab150075; Abcam and Alexa Fluor 488 goat anti-mouse IgG, 1:200, ab150133; Abcam) were used and incubated for 2 h. After each antibody incubation, the samples were washed 6 times with PBST (containing 0.05% Tween 20) for 10 min. For liquid staining, the BODIPY493/503 dye was incubated overnight at 4°C. Nuclear staining was performed via incubation with DAPI for 10 min. Images were obtained by CLSM.

Transfection of lentivirus

Chondrocytes were cultured to 30%–50% confluence in 10% FBS DMEM and then transfected with lentivirus carrying *Plin1* (Hanbio) at a final concentration of 30 MOI (multiplicity of infection) according to the manufacturer's instructions. The carrier of the *Plin1* gene was pHBLV-CMV-MCS-3FLAG-EF1-ZsGreen-T2A-PURO. The gene and lentivirus information is shown in Table S3. We used the one-half infection method for infection. Briefly, only half of the fresh complete medium was added at the time of lentivirus infection, and the medium was replenished 4 h later. When we performed lentivirus transfection, we also used 5 μg/mL polybrene (Hanbio) to aid in transfection according to the manufacturer's instructions. The chondrocytes were infected for 72 h before testing. We used GFP tracing by CLSM and western blot analysis to measure the transfection efficiency. In addition, owing to the 488 nm GFP carried by the lentivirus, we used another neutral lipid droplet stain kit, HCS LipidTOX™ Deep Red neutral lipid Stain (H34477; Thermo Fisher Scientific) to observe neutral LDs.

Statistical analysis

The results were based on three replications and analyzed using GraphPad Prism 9.0.0 software (GraphPad Software Inc., San Diego, USA). Two-tailed Student's *t* test for two groups and one-way analysis of variance for multiple groups were used to test differences. Differences were considered statistically significant at $P < 0.05$.

Results

FGF8 promotes lipid droplet accumulation in chondrocytes

To investigate the effect of FGF8 on chondrocyte metabolism, we performed RNA sequencing on chondrocytes exposed to FGF8 at 25 ng/mL for 24 h. We clustered all the altered pathways via KEGG analysis and found that multiple lipid metabolism-related pathways, such as fat absorption and digestion, ether lipid metabolism, glycosphingolipid biosynthesis, regulation of lipolysis in adipocytes, the PPAR signaling pathway, and arachidonic acid metabolism pathways, were upregulated (Figure 1A, red boxes). These upregulated signaling pathways are tightly correlated with lipid abundance and distribution [54,55] and indicate potential changes in LDs in chondrocytes after FGF8 treatment. To visualize the changes in neutral lipid and LD accumulation in chondrocytes, we performed fluorescence staining using BODIPY493/503 in chondrocytes exposed to FGF8 at 25, 50, and 100 ng/mL (Figure 1B at high magnification and Supplementary Figure S1 at low magnification) and found that FGF8 significantly increased neutral lipid accumulation by increasing the number of LDs formed. Total fluorescence quantification confirmed the increase in the number of neutral LDs

in the chondrocytes (Figure 1C). In addition, quantification of the number of visible LDs further confirmed that FGF8 increased the accumulation of neutral lipids and LDs in chondrocytes (Figure 1D). By injecting an adeno-associated virus (AAV) carrying the *FGF8* gene into the mouse temporomandibular joint to achieve *FGF8* overexpression in cartilage tissue, we found that neutral lipid and LD accumulation was largely enhanced (Figure 1E). We observed that neutral lipid accumulation was increased in both the proliferative layer (white arrows, boxed area) and the hypertrophic layer (yellow arrows, boxed area). By quantifying the neutral lipids in the entire cartilage layer, we confirmed the increase in neutral lipid accumulation in cartilage induced by FGF8 (Figure 1F).

FGF8 promotes lipid droplet accumulation by upregulating Plin1 in chondrocytes

To explore how FGF8 promotes LD accumulation in chondrocytes, we clustered differentially expressed gene candidates that were tightly correlated with LD maturation on the basis of RNA sequencing in the form of a pheatmap (Figure 2A). Through protein-protein interaction analysis using STRING (Supplementary Figure S2), we established an interaction network among these candidates for FGF8-mediated LD accumulation. Notably, we found that the expression of Plin1, which plays a major role in LD formation and maturation by enveloping LDs to protect them against breakdown [20], was significantly increased in chondrocytes exposed to 25 ng/mL FGF8 (red box). qPCR was then performed to confirm the *Plin1* gene change in chondrocytes exposed to 25 ng/mL FGF8 and FGF8 was found to increase the gene expression of *Plin1* up to 1.85-fold relative to that in the control group (Figure 2B). At the protein level, western blot analysis showed that the expression of Plin1 increased in chondrocytes induced by FGF8 (Figure 2C), and quantitative analysis of the Plin1 protein confirmed this result (Figure 2D). We also detected protein changes in hormone-sensitive lipase (HSL), diacylglycerol O-acyltransferase 2 (DGAT2), and adipose triglyceride lipase (ATGL) in chondrocytes induced by FGF8 (Supplementary Figure S3) and found that HSL was significantly decreased. Next, we performed immunofluorescence analysis to explore the protein expression and distribution of Plin1 in chondrocytes exposed to FGF8 (Figure 2E). The results revealed that Plin1 was distributed mainly in the cytoplasm around the nucleus and that its expression increased in chondrocytes in response to 25 ng/mL FGF8. Using total fluorescence quantification, we further confirmed the increase in Plin1 expression in chondrocytes (Figure 2F). In addition, in the cartilage layer, we detected increased Plin1 expression induced by AAV-FGF8 overexpression (Supplementary Figure S4). RNA interference was performed to verify the importance of Plin1 in FGF8-mediated LD accumulation. After confirming the knockdown efficiency of 50 nM si-Plin1 (Figure 2G), we performed immunofluorescence staining (Figure 2H at high magnification and Supplementary Figure S5 at low magnification), and the results revealed that the knockdown of *Plin1* clearly reduced LD accumulation in chondrocytes exposed to FGF8. Total fluorescence quantification further confirmed the reduced protein expression of Plin1 in chondrocytes caused by RNA interference in the presence of FGF8 (Figure 2I). Quantification of the number of visible LDs (Figure 2J) and total fluorescence per cell (Supplementary Figure S6) confirmed the changes in LDs in chondrocytes induced by si-Plin1 in the presence of FGF8. Furthermore, we overexpressed Plin1 via lentivirus transfection to determine the effect of Plin1 overexpression on LD accumulation. First, we used CLSM to detect the efficiency of Plin1 overexpression in chondrocytes at an MOI of 30 and found that the lentivirus carrying *Plin1* was successfully transfected into the chondrocytes (Supplementary Figure S7). At the protein level, immunofluorescence staining confirmed the overexpression of Plin1 in chondrocytes after lentivirus transfection (Figure 2L), and total fluorescence quantification verified the increase in Plin1 protein in chondrocytes (Figure 2M). Using western blot analysis, we confirmed that the expression of Plin1 in chondrocytes after Plin1 overexpression was approximately 2-*fold* higher than that in the vector control (Figure 2N,O). After confirming the overexpression efficiency of LVs, we next investigated LD accumulation in chondrocytes after Plin1 overexpression (Figure 2P and Supplementary Figure S8). The results showed that overexpression of Plin1 significantly promoted LD accumulation in chondrocytes. Quantification of the number of visible LDs (Figure 2) Qand total fluorescence of lipids per cell (Supplementary Figure S9) confirmed that these changes in chondrocytes were induced by Plin1 overexpression. Taken together, these results demonstrate that FGF8 enhances LD accumulation by increasing the expression of Plin1 in chondrocytes (Figure 2K).

FGF8-mediated lipid droplet accumulation requires the participation of FGF receptor 1 (FGFR1)

To explore how FGF8 enters chondrocytes to initiate downstream responses, we clustered the differentially expressed FGF receptors via RNA sequencing and found that only FGFR1 was upregulated in chondrocytes treated with 25 ng/ml FGF8 (Figure 3A and Supplementary Figure S10). We then performed qPCR to confirm the increased gene expression of *FGFR1* in chondrocytes (Figure 3B). To determine the role of FGFR1 in FGF8-mediated LD accumulation in chondrocytes, we used the siRNA targeting *FGFR1*. After confirming the knockdown efficiency of 50 nM si-FGFR1 (Figure 3C), we detected the gene expression of *Plin1* via qPCR (Figure 3D), and the results revealed that si-FGFR1 strongly decreased the increase in *Plin1* gene expression in chondrocytes exposed to FGF8. Using immunofluorescence, we observed that si-FGFR1 effectively impaired the increase in cytoplasmic Plin1 protein level in chondrocytes exposed to FGF8 (Figure 3E). Fluorescence quantification confirmed this reduction (Figure 3F). We next investigated changes in LD accumulation in chondrocytes induced by si-FGFR1 in the presence of FGF8 (Figure 3G), and the results revealed that LD accumulation was significantly lower in chondrocytes treated with si-FGFR1 than in those treated with FGF8. Quantification of the number of visible LDs (Figure 3H) and total fluorescence intensity (Supplementary Figure S11) further confirmed the changes in LD accumulation in chondrocytes treated with si-FGFR1 in the presence of FGF8.

FGF8 activates p-p38 signaling in chondrocytes

To further determine which cytoplasmic signaling pathway is activated in chondrocytes exposed to FGF8, we first performed western blot analysis (Figure 4A) and found that FGF8 increased the expression of p-Erk (up to 1.5-fold) and p-p38 (up to 3.0-fold) relative to that in the control groups (Figure 4B). Given that the change in p-p38 expression was greater than that in p-Erk expression in chondrocytes exposed to FGF8, we focused on the role of p-p38 signaling in FGF8-mediated LD accumulation.

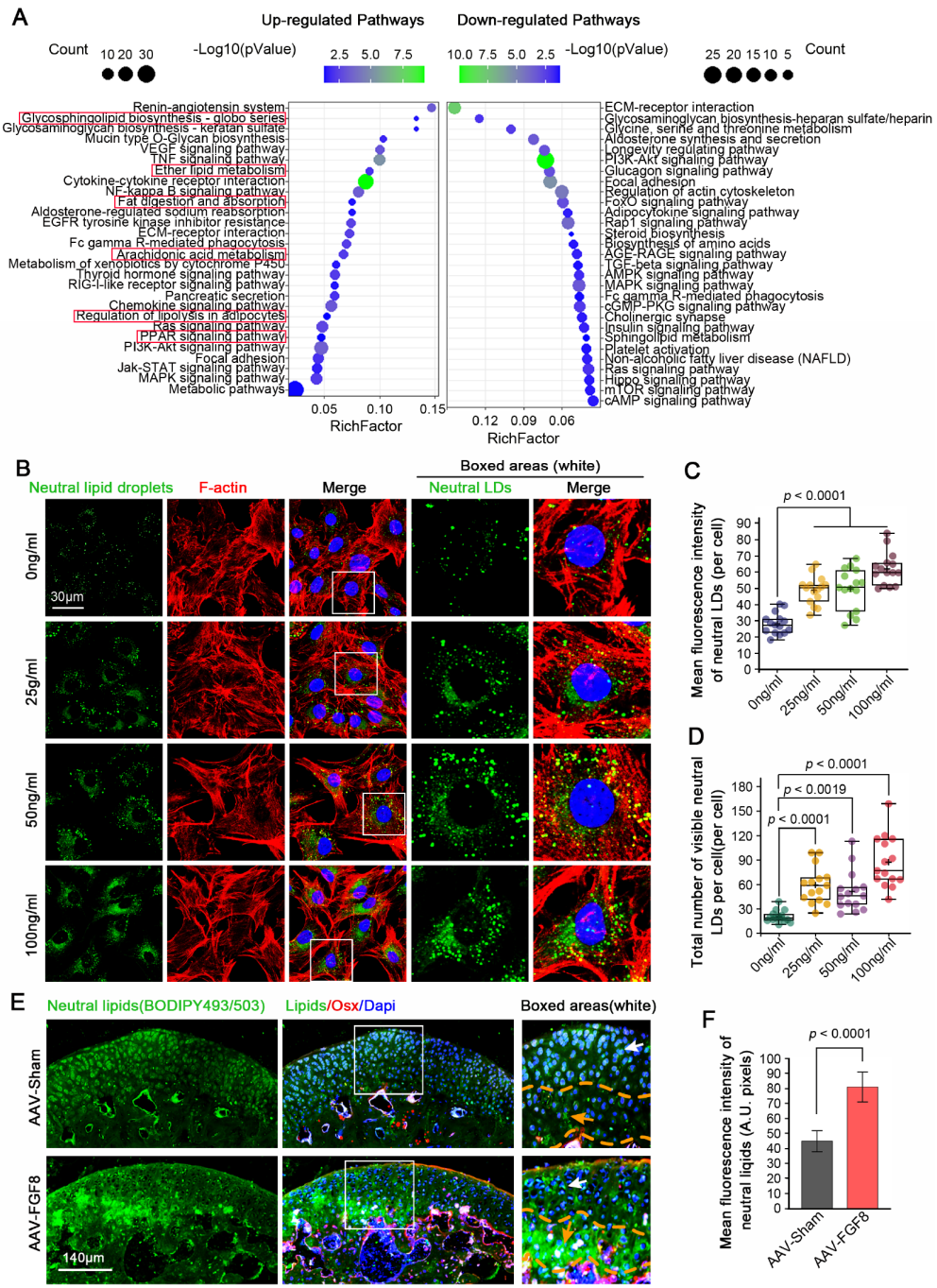

Figure 1. FGF8 induces lipid droplet accumulation in chondrocytes (A) KEGG analysis based on RNA sequencing data showing changes in signaling pathways in chondrocytes exposed to FGF8 at 25 ng/mL. The left side indicates upregulated pathways, and the right side indicates downregulated pathways. The red boxes refer to the signaling pathways closely associated with lipid droplet accumulation. (B) Representative fluorescence images showing changes in lipid droplets in chondrocytes exposed to different concentrations of FGF8. Chondrocytes were treated with FGF8 at 0, 25, 50, and 100 ng/mL for 2 days and then imaged using a 60× CLSM. Green fluorescence indicates lipids, red fluorescence indicates the cytoskeleton (F-actin), and blue fluorescence indicates the nuclei. The white dashed boxes indicate the magnified regions. (C) Total fluorescence quantification per cell confirming changes in lipid accumulation in chondrocytes treated with 0, 25, 50, or 100 ng/mL FGF8 for 2 days. The data were based on 15 cells from three independent samples (n = 3). (D) Quantification of the number of visible lipid droplets per cell, confirming the changes in the number of lipid droplets in chondrocytes exposed to 0, 25, 50, and 100 ng/mL FGF8 for two days. The data were based on 15 cells from three independent samples (n = 3). (E) Representative fluorescence images showing changes in lipid accumulation in cartilage caused by AAV-FGF8 overexpression. Green fluorescence indicates lipids, red fluorescence indicates Osx staining (negative in mature cartilage and positive in calcified cartilage), and blue fluorescence indicates the nuclei. The white dashed boxes indicate the magnified regions. (F) Quantification of the mean fluorescence intensity confirming the changes in lipid accumulation in the cartilage exposed to FGF8. The data were based on three replications (n = 3). The data in (C, D and F) were analyzed via one-way analysis of variance. The data in (C and D) were shown in box (from 25%, 50% to 75%) and whisker (minimum to maximum) plots. Differences were considered statistically significant at $P < 0.05$.

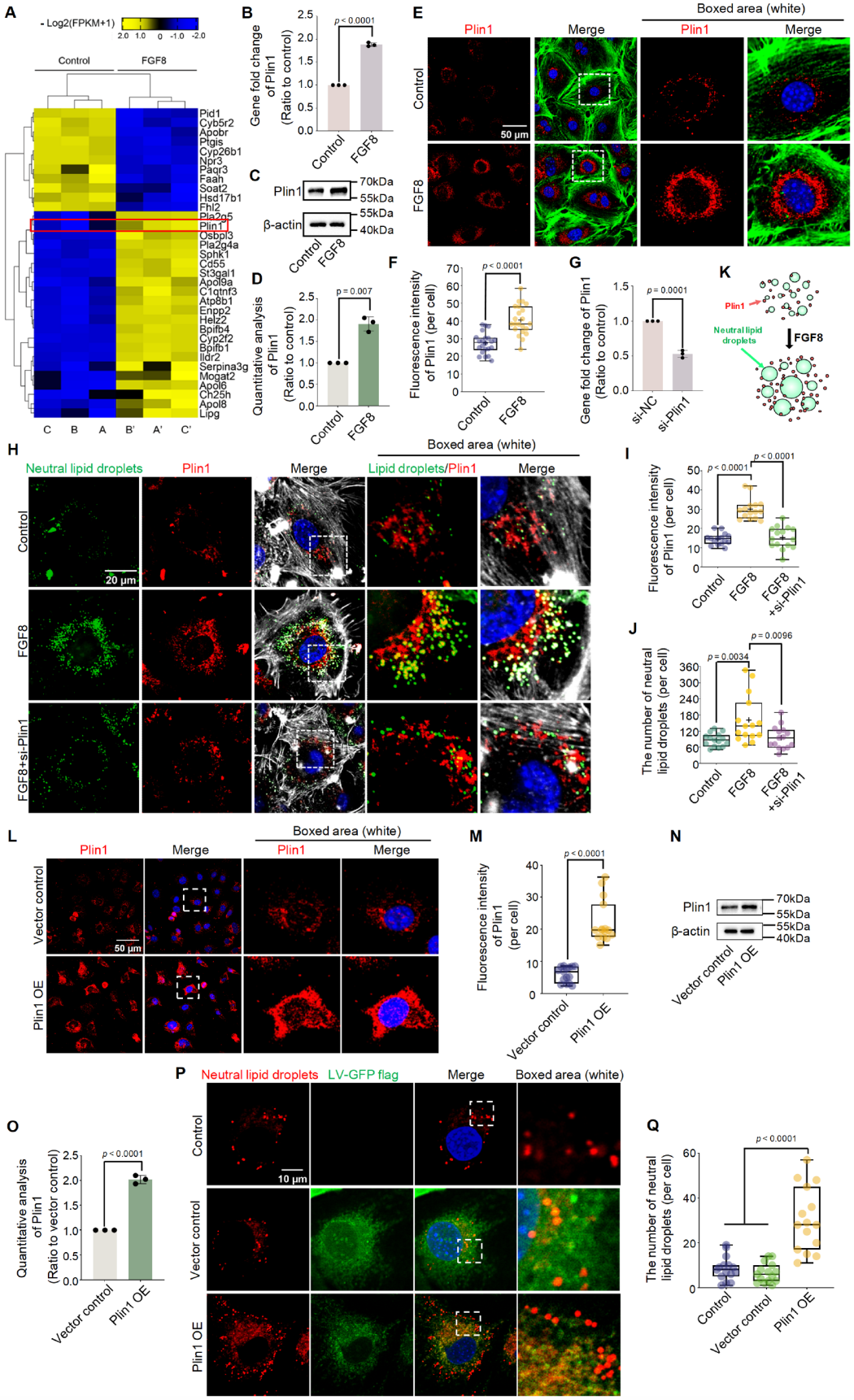
A
Log2(FPKM+1)
Control
FGF8
Pid1
Cyb5r2
Apobr
Ptgis
Cyp26b1
Npr3
Paqr3
Faah
Soat2
Hsd17b1
Fhl2
Pla2g5
Plin1
Osbpl3
Pla2g4a
Sphk1
Cd55
St3gal1
Apol9a
C1qtnf3
Atp8b1
Enpp2
Helz2
Bpifb4
Cyp2f2
Bpifb1
Ildr2
Serpina3g
Mogat2
Apol6
Ch25h
Apol8
Lipg
C B A B' A' C'
B
Gene fold change of Plin1 (Ratio to control)
p < 0.0001
Control
FGF8
C
Plin1
β-actin
70kDa
55kDa
55kDa
40kDa
D
Quantitative analysis of Plin1 (Ratio to control)
p = 0.007
E
Plin1
Merge
Boxed area (white)
50 μm
F
Fluorescence intensity of Plin1 (per cell)
p < 0.0001
G
Gene fold change of Plin1 (Ratio to control)
p = 0.0001
si-NC
si-Plin1
K
Plin1
Neutral lipid droplets
FGF8
H
Neutral lipid droplets
Lipid droplets/Plin1
20 μm
FGF8+si-Plin1
I
p < 0.0001
FGF8 +si-Plin1
J
p = 0.0096
p = 0.0034
The number of neutral lipid droplets (per cell)
L
Vector control
Plin1 OE
M
N
O
Vector control
Plin1 OE
P
LV-GFP flag
10 μm
Q

Figure 2. FGF8 enhances lipid droplet accumulation by upregulating Plin1 in chondrocytes (A) The pheatmap based on RNA sequencing indicating changes in the levels of candidate mediators involved in lipid droplet accumulation. The red box indicates the gene changes in *Plin1*. Chondrocyte samples A & A', B & B', and C & C' were three groups of independent samples. The gene candidates are presented as –log2(1+FPKM) values and are generated using the online R package FPKM, Fragments Per Kilobase of exon model per million mapped fragments. (B) qPCR verifying the change in Plin1 expression in chondrocytes exposed to FGF8 at 25 ng/mL. The data were based on three replications (n = 3). (C) Western blot analysis showing the upregulation of Plin1 in chondrocytes induced by FGF8. β-Actin was used as the internal reference. Data were representative of three independent samples (n = 3). (D) Quantitative analysis confirming the fold change in Plin1 protein expression in chondrocytes treated with FGF8 in (C). The data were based on three replicates (n = 3). (E) Representative fluorescence images showing changes in Plin1 in chondrocytes exposed to 25 ng/mL FGF8. Fluorescence images were captured via CLSM at 60× magnification. Red fluorescence indicates Plin1, green fluorescence indicates the cytoskeleton (F-actin), and blue fluorescence indicates the nuclei. The white dashed boxes indicate the magnified regions. (F) Total fluorescence quantification per cell confirming the changes in Plin1 protein levels in (E) chondrocytes treated with FGF8 at 25 ng/mL. The data were based on 21 cells from three independent samples (n = 3). (G) qPCR was used to verify the knockdown efficiency of 50 nM si-Plin1 in chondrocytes. The data were based on three replicates (n = 3). (H) Representative fluorescence images of individual cells indicating changes in lipid droplets in chondrocytes exposed to si-Plin1 in the presence of FGF8 at 25 ng/mL. Chondrocytes were pretreated with siRNA for 12 h and then treated with FGF8 at 25 ng/mL for 2 days. Fluorescence images were obtained using 60× CLSM. Green fluorescence indicates lipid droplets, red fluorescence indicates Plin1, gray fluorescence indicates the cytoskeleton (F-actin), and blue fluorescence indicates the nuclei. The white dashed boxes indicate the magnified regions. (I) Total fluorescence quantification per cell confirming the changes in Plin1 protein in (F) chondrocytes exposed to si-Plin1 in the presence of FGF8. The data were based on 15 cells from three independent samples (n = 3). (J) Quantification of the number of visible lipid droplets per cell confirming the changes in the number of lipid droplets in chondrocytes inhibited by si-Plin1 in the presence of FGF8 at 25 ng/mL. The data were based on 15 cells from three independent samples (n = 3). (K) Schematic diagram showing that Plin1 protects against the breakdown of lipid droplets and promotes the formation of larger lipid droplets in the presence of FGF8. (L) Representative fluorescence images showing changes in Plin1 in chondrocytes after Plin1 overexpression by lentivirus. Fluorescence images were obtained using 60× CLSM. Red fluorescence indicates Plin1, and blue fluorescence indicates the nuclei. The white dashed boxes indicate the magnified regions. (M) Total fluorescence quantification per cell confirming the change in Plin1 protein levels in the chondrocytes in (L). The data were based on 15 cells from three independent samples (n = 3). (N) Western blot analysis showing increased expression of Plin1 in chondrocytes after Plin1 overexpression by lentivirus. β-Actin was used as the internal reference. Data were representative of three independent samples (n = 3). (O) Quantitative analysis confirming the fold change in Plin1 protein expression in the chondrocytes in (N). The data were based on three independent samples (n = 3). (P) Representative fluorescence images of individual cells showing changes in lipid droplets in chondrocytes after Plin1 overexpression by lentivirus. Fluorescence images were obtained using CLSM (60×). Green fluorescence indicates the GFP carried by the lentivirus, red fluorescence indicates lipid droplets, and blue fluorescence indicates the nuclei. The white dashed boxes indicate the magnified regions. (Q) Quantification of the number of visible lipid droplets per cell confirming the changes in lipid droplet accumulation in the chondrocytes in (P). The data were based on 15 cells from three independent samples (n = 3). The data in (F, I, J, M, N, and Q) were analyzed using one-way analysis of variance. The data in (B, D, G, M, O, and Q) were analyzed using two-tailed Student's t tests. The data in (B, D, G, and O) were presented as the mean ± SD. The data in (F, I, M and Q) were shown in the box (from 25%, 50% to 75%) and whisker (minimum to maximum) plots. Differences were considered statistically significant at $P < 0.05$.

Immunofluorescence staining was used to detect the cytoplasmic expression and distribution of p-p38 in chondrocytes exposed to FGF8 (Figure 4C), and the results revealed that FGF8 increased the protein expression of p-p38. More importantly, the increase in p-p38 was highly concentrated in the nuclear region of chondrocytes treated with FGF8 at 25 ng/mL (Figure 4C, boxed areas). Using total fluorescence quantification per cell (Figure 4D) and linear fluorescence quantification in the nuclear region (Figure 4E), we further confirmed the increase in p-p38 in chondrocytes exposed to FGF8.

FGF8 promotes lipid droplet accumulation via the FGFR1/p-p38 axis

To confirm the role of p-p38 signaling in FGF8-mediated LD accumulation, we used SB203580, a specific inhibitor of p-p38 [56]. Western blot analysis confirmed that SB203580 effectively reduced the upregulation of p-p38 in chondrocytes induced by FGF8 (Figure 5A,B). Immunofluorescence staining was used to detect the cytoplasmic expression of p-p38 in chondrocytes exposed to FGF8 (Figure 5C), and the results showed that SB203580 treatment significantly reduced the expression of p-p38 in chondrocytes in the presence of FGF8. The total fluorescence quantification per cell (Figure 5D) and linear fluorescence quantification in the nuclear region (Figure 5E) further confirmed this reduction, thus confirming the effectiveness of blocking p-p38 in chondrocytes. We then investigated the expression of Plin1 in chondrocytes treated with SB203580 in the presence of FGF8 (Figure 5F–H). qPCR revealed that the gene expression of *Plin1* was decreased in chondrocytes with p-p38 blockade in the presence of FGF8 compared with that in the individual FGF8-treated group (Figure 5F). Using immunofluorescence staining, we observed that blocking p-p38 with SB203580 effectively reduced the cytoplasmic expression of Plin1 protein in the presence of FGF8 (Figure 5G), and total fluorescence quantification per cell confirmed this reduction (Figure 5H). We detected LD accumulation in chondrocytes treated with SB203580 in the presence of FGF8. Using immunofluorescence staining, we observed that LD accumulation was significantly reduced in chondrocytes treated with SB203580 in the presence of FGF8 relative to that in the individual FGF8-treated group (Figure 5I). Quantification of the number of visible LDs (Figure 5J) and total fluorescence intensity (Supplementary Figure S12) further confirmed the changes in LD accumulation in chondrocytes treated with SB203580 in the presence of FGF8.

To determine the regulatory correlation between FGFR1 and p-p38 in chondrocytes exposed to FGF8, we detected the expression of p-p38 signaling in chondrocytes via siRNA targeting *FGFR1* in the presence of FGF8. By western blot analysis, we observed that knockdown of *FGFR1* significantly decreased the protein expression of p-p38 in chondrocytes in the presence of FGF8 (Figure 6A,B). Using immunofluorescence staining, we found that si-FGFR1 reduced the protein expression and nuclear accumulation of p-p38 in chondrocytes in the presence of FGF8 (Figure 6C). Total fluorescence quantification (Figure 6D) and linear fluorescence quantification of p-p38 in the nuclear region (Figure 6E) further confirmed this result.

Collectively, these results indicate that FGF8 promotes LD accumulation in chondrocytes mainly via the FGFR1/p38 axis.

Discussion

As the only cell type in cartilage, chondrocytes exhibit abundant

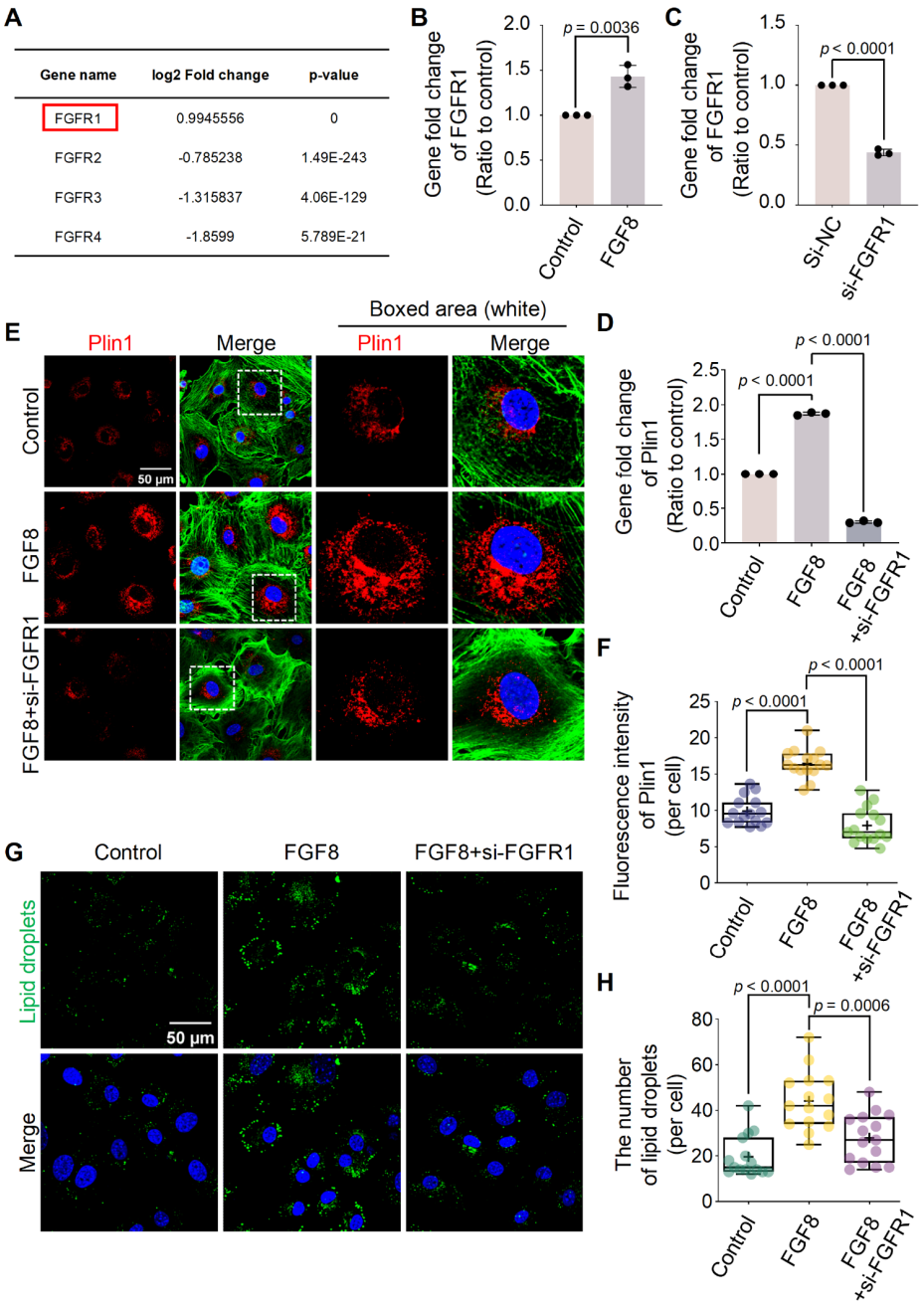

Figure 3. FGF8 enhances lipid droplet accumulation in chondrocytes via FGFR1 (A) RNA sequencing data showing changes in the gene expression of *FGFRs* in chondrocytes exposed to 25 ng/mL FGF8. The red box indicates upregulated FGFR1 expression. (B) qPCR verifying the expression of *FGFR1* in chondrocytes exposed to FGF8 at 25 ng/mL. The data were based on three independent repetitions (n = 3). (C) qPCR verifying the knockdown efficiency of 50 nM si-FGFR1 in chondrocytes. The data were based on three independent experiments (n = 3). (D) qPCR was used to verify the decreased expression of *Plin1* in chondrocytes induced by si-FGFR1 in the presence of FGF8. Chondrocytes were pretreated with siRNA for 12 h and then treated with FGF8 (25 ng/mL) for 12 h. The data were based on three independent experiments (n = 3). (E) Representative fluorescence images showing the expression of Plin1 in chondrocytes exposed to si-FGFR1 in the presence of FGF8. Chondrocytes were pretreated with siRNA for 12 h and then treated with FGF8 at 25 ng/mL for 2 days. The images were captured using 60× CLSM. Red fluorescence indicates Plin1, green fluorescence indicates the cytoskeleton (F-actin), and blue fluorescence indicates the nuclei. The white dashed boxes indicate the magnified regions. (F) Total fluorescence quantification per cell, confirming the decrease in Plin1 protein in chondrocytes caused by si-FGFR1 in the presence of FGF8 at 25 ng/mL. The data were based on 15 cells from three independent samples (n = 3). (G) Representative fluorescence images (60×) showing the change in lipid droplet accumulation in chondrocytes exposed to si-FGFR1 in the presence of FGF8 at 25 ng/mL. Green indicates lipid droplets, and blue indicates nuclei. (H) Quantification of the number of visible lipid droplets per cell confirming the changes in the number of lipid droplets in chondrocytes exposed to si-FGFR1 in the presence of FGF8 at 25 ng/mL. The data were based on 15 cells from three independent replicates (n = 3). The data in (B and C) were analyzed using two-tailed Student's t tests. The data in (D, F, and H) were analyzed using one-way analysis of variance. The data in (B, C, and D) were presented as the mean ± SD. The data in (F and H) were shown in box (25%, 50% to 75%) and whisker (minimum to maximum) plots. Differences were considered statistically significant at $P < 0.05$.

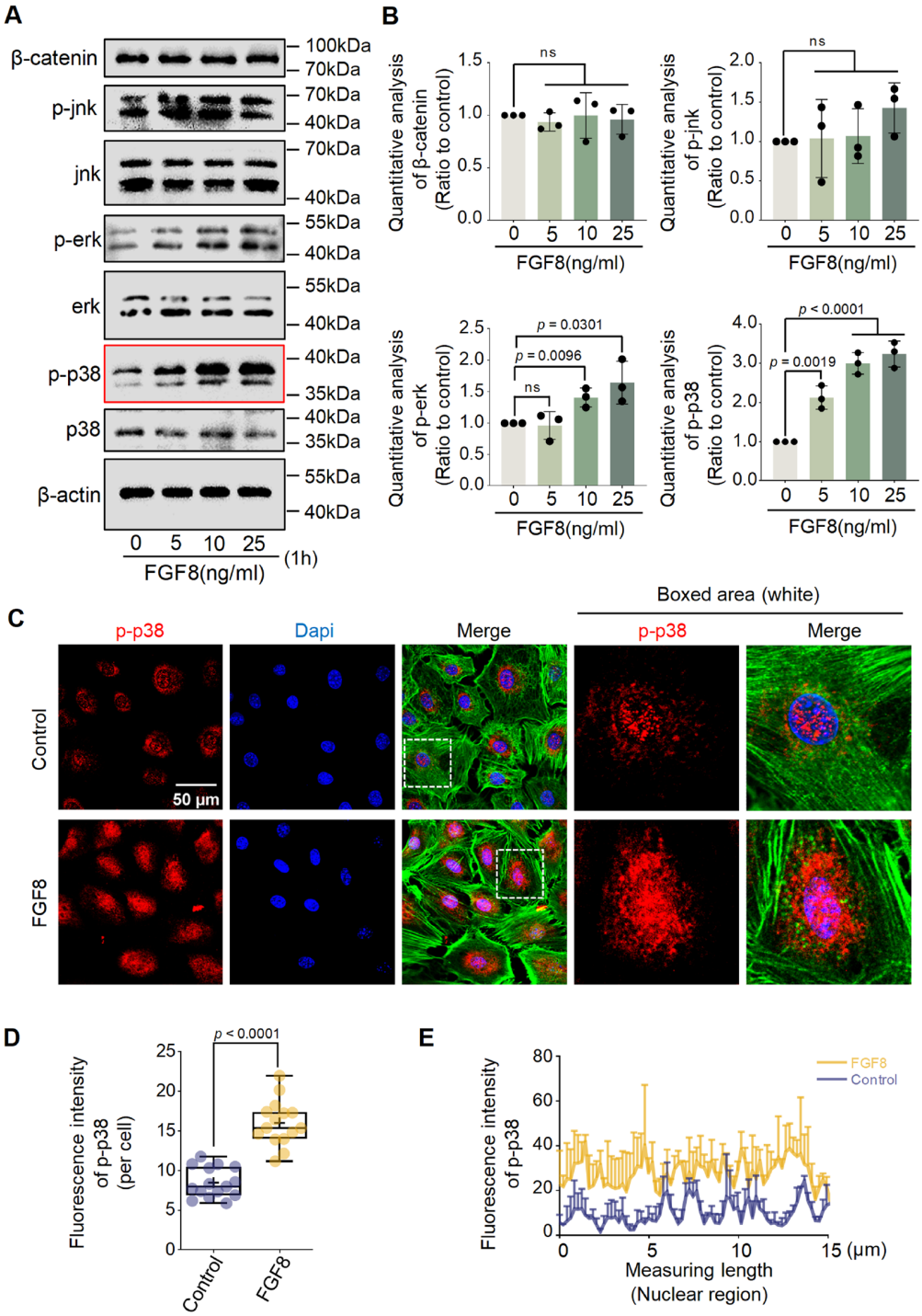

Figure 4. FGF8 activates p-p38 signaling in chondrocytes (A) Western blot analysis showing the upregulation of p-p38 signaling in chondrocytes exposed to different concentrations of FGF8. β-Actin was used as the internal reference. The cell lysates were collected after treatment with FGF8 for 1 h. The red box shows the change in p-p38 signaling. The data were representative of three independent samples ($n = 3$). (B) Quantitative analysis confirming the fold change in p-p38 protein expression in chondrocytes treated with FGF8 in (A). The data were based on three replicates ($n = 3$). (C) Representative fluorescence images (60×) showing the change in p-p38 in chondrocytes exposed to FGF8 at 25 ng/ml for 1 h. Red fluorescence indicates p-p38, green fluorescence indicates the cytoskeleton (F-actin), and blue fluorescence indicates the nuclei. The white dashed boxes indicate the magnified regions. (D) Total fluorescence quantification per cell confirming the change in p-p38 protein levels in chondrocytes exposed to FGF8 at 25 ng/mL for 1 h. The data were based on 15 cells from three independent samples ($n = 3$). (E) Representative linear fluorescence quantification of chondrocyte nuclei showing a change in p-p38 after exposure to FGF8 at 25 ng/mL. The average nuclear diameter ranged from 8 to 15 μm. The data were based on three independent replicates ($n = 3$). The data in (B) were analyzed via one-way analysis of variance. The data in (D) were analyzed via two-tailed Student's *t* tests. The data in (B) are presented as the mean ± SD. The data in (D) are shown in box (from 25%, 50% to 75%) and whisker (minimum to maximum) plots. Differences were considered statistically significant at $P < 0.05$.

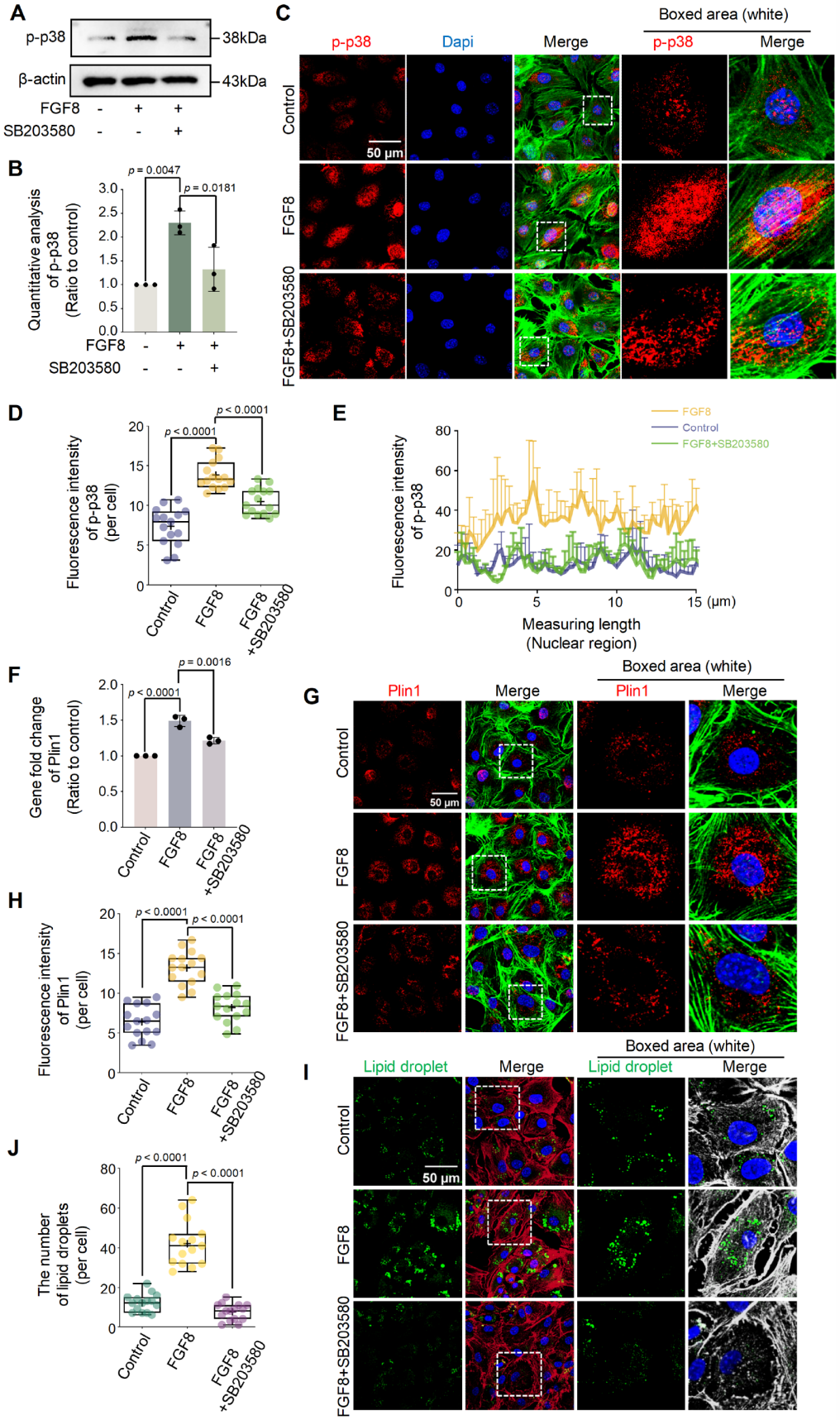
A
p-p38
38kDa
β-actin
43kDa
FGF8 - + +
SB203580 - - +
B
Quantitative analysis of p-p38 (Ratio to control)
p = 0.0047
p = 0.0181
FGF8 - + +
SB203580 - - +
C
Boxed area (white)
p-p38
Dapi
Merge
p-p38
Merge
Control
FGF8
FGF8+SB203580
50 μm
D
Fluorescence intensity of p-p38 (per cell)
p < 0.0001
p < 0.0001
Control
FGF8
FGF8 +SB203580
E
Fluorescence intensity of p-p38
FGF8
Control
FGF8+SB203580
Measuring length (Nuclear region)
15 (μm)
F
Gene fold change of Plin1 (Ratio to control)
p = 0.0016
p < 0.0001
Control
FGF8
FGF8 +SB203580
G
Boxed area (white)
Plin1
Merge
Plin1
Merge
Control
FGF8
FGF8+SB203580
50 μm
H
Fluorescence intensity of Plin1 (per cell)
p < 0.0001
p < 0.0001
Control
FGF8
FGF8 +SB203580
I
Boxed area (white)
Lipid droplet
Merge
Lipid droplet
Merge
Control
FGF8
FGF8+SB203580
50 μm
J
The number of lipid droplets (per cell)
p < 0.0001
p < 0.0001
Control
FGF8
FGF8 +SB203580

Figure 5. FGF8 promotes lipid droplet accumulation in chondrocytes through p-p38 signaling (A) Western blot analysis showing that the expression of p-p38 in chondrocytes was inhibited by SB203580 in the presence of FGF8. Chondrocytes were pretreated with SB203580 at 20 μM for 1 h and then treated with FGF8 at 25 ng/mL. β-Actin was used as the internal reference. (B) Quantitative analysis confirming the change in p-p38 signaling in the chondrocytes in (A). The data were based on three replicates ($n = 3$). (C) Representative fluorescence images showing p-p38 protein expression in chondrocytes exposed to SB203580 in the presence of FGF8. Chondrocytes were pretreated with SB203580 at 20 μM for 1 h and then treated with FGF8 at 25 ng/mL. The images were captured using CLSM (60×). Red fluorescence indicates Plin1, green fluorescence indicates the cytoskeleton (F-actin), and blue fluorescence indicates the nuclei. The white dashed boxes indicate the magnified regions. (D) Total fluorescence quantification per cell showing the change in p-p38 in chondrocytes exposed to SB203580 in the presence of FGF8 at 25 ng/mL. The data were based on 15 cells from three independent samples ($n = 3$). (E) Representative linear fluorescence quantification of chondrocyte nuclei showing the change in the nuclear accumulation of p-p38 in chondrocytes inhibited by SB203580 in the presence of 25 ng/mL FGF8. The average nuclear length was in the range of 8-15 μm. The data were based on three replicates ($n = 3$). (F) qPCR showing the change in the gene expression of *Plin1* in chondrocytes exposed to SB203580 in the presence of FGF8. Chondrocytes were pretreated with SB203580 at 20 μM for 1 h and then treated with FGF8 at 25 ng/mL for 12 h. Data were obtained from three replicates ($n = 3$). (G) Representative fluorescence images showing the change in Plin1 expression in chondrocytes exposed to SB203580 in the presence of FGF8 at 25 ng/mL. The images were obtained via CLSM (60×). Red fluorescence indicates Plin1, green fluorescence indicates the cytoskeleton (F-actin), and blue fluorescence indicates the nuclei. The white dashed boxes show the magnified regions. (H) Total fluorescence quantification per cell confirming the change in Plin1 in chondrocytes induced by SB203580 in the presence of FGF8 at 25 ng/mL. The data were based on 15 cells from three independent samples ($n = 3$). (I) Representative fluorescence images showing the change in lipid droplets in chondrocytes induced by SB203580 in the presence of FGF8 at 25 ng/mL. Images were captured using CLSM (60 ×). Green fluorescence indicates lipid droplets, red fluorescence indicates the cytoskeleton (F-actin), and blue fluorescence indicates the nuclei. The white dashed boxes indicate the magnified regions. (J) Quantification of the number of visible lipid droplets per cell showing the change in the number of lipid droplets in chondrocytes induced by SB203580 in the presence of 25 ng/mL FGF8. The data were based on 15 cells from three independent samples ($n = 3$). The data in (B, D, F, H, and J) were analyzed via one-way analysis of variance. The data in (B and F) are presented as the mean ± SD. The data in (D, H, and J) are shown in the box (from 25%, 50% to 75%) and whisker (minimum to maximum) plots. Differences were considered statistically significant at $P < 0.05$.

lipid deposition and LD accumulation [36]. LD accumulation and metabolism are influenced by various biochemical factors [42,43]. FGF8, one of the most important biochemical factors that can modulate the proliferation, differentiation, migration, and metabolism of chondrocytes, has attracted increasing attention in the physiology and pathology of cartilage [44,57]. To date, no study has explored the importance of FGF8 in LD accumulation in chondrocytes. Here, we showed that FGF8 promotes LD accumulation in chondrocytes by upregulating the Plin1 protein and that FGF8-mediated LD accumulation occurs mainly through the FGFR1/p-p38 axis (Figure 7). These results expand our understanding of how cellular lipid metabolic homeostasis is remodeled by biochemical factors.

Owing to the nutrient-limited microenvironment without the supply of blood vessels, lymphatic vessels and nerves, cartilage obtains nutrients from surrounding tissues through diffusion [24,26,58], and its metabolism is thus greatly influenced by neighboring signals [59]. The synovium, a thin layer of connective tissue, provides a nonadherent surface for joint cartilage and secretes paracrine factors that influence articular chondrocyte metabolism [59,60]. We previously showed that crosstalk with osteoblasts from subchondral bone also increases cartilage lipid catabolism by impairing cholesterol synthesis and accumulation [61] and induces glucose-derived ATP perturbations in chondrocytes [62]. Physiologically, chondrocytes must effectively utilize diffuse nutrients, including lipids, to meet energy needs and thus maintain cellular activities such as signal transmission, protein synthesis, resting potential maintenance, and DNA replication and repair [34]. From a disease perspective, abnormal lipid accumulation in chondrocytes has been associated with a variety of osteoarticular diseases, including OA [37,63]. For example, Park *et al.* [30] reported that LD accumulation within chondrocytes induced by PPARα and ACOT12 deficiency accelerates the degeneration of the cartilage matrix in OA. Wang *et al.* [31] reported that GDF11 inhibits abnormal lipid formation and LD accumulation by promoting the ubiquitination of PPARγ in chondrocytes in temporomandibular joint osteoarthritis. Moreover, as a typical inflammatory disease, OA progression is accompanied by significant upregulation of cytokines, including FGF8, in the joint cavity [44]. Here, we found that FGF8 upregulates multiple lipid metabolism-related pathways, such as fat absorption and digestion, ether lipid metabolism, and arachidonic acid metabolism pathways (Figure 1A), and facilitates LD accumulation in chondrocytes (Figure 1B–F and Supplementary Figure S1). Overall, the increase in lipid accumulation in chondrocytes caused by FGF8 may explain lipid accumulation and pathological deterioration in osteoarthritic cartilage [47,64,65].

Plin family members, including Plin1-5, are the main modulators of LD accumulation [20]. Compared with other members, Plin1 is a more extensively studied protein that is thought to be responsible for LD accumulation [12]. For example, Wei *et al.* [66] reported that overexpression of Plin1 blocks LD degradation and promotes abnormal LD growth. Sun *et al.* [67] showed that Plin1 promotes unilocular lipid droplet formation through the activation of Fsp27 in adipocytes. Wang *et al.* [68] found that Plin1 forms a complex with apol6, which prevents Plin1 from binding to HSL, thereby inhibiting lipolysis and increasing LD accumulation. Under normal physiological conditions, Plin1 is located on the surface of LDs via its hydrophobic structural domains and binds to α/β-hydrolase domain-containing protein 5 (ABHD5) to inhibit phospholipid lipolysis, thereby promoting LD formation and enlargement [20]. Conversely, during intracellular lipolysis, Plin1 undergoes phosphorylation and facilitates the release of phosphorylated ABHD5. Phosphorylated ABHD5 combines with phosphorylated ATGL to further increase lipolysis [20]. In addition, phosphorylated Plin1 recruits and binds to HSL to increase lipolysis [20]. For example, Cao *et al.* [64] reported that with a high-fat diet, Plin1 could be phosphorylated by adenylate cyclase 7 and promote inflammatory lipolysis of LDs in fibroblast-like synoviocytes, exacerbating OA. By knocking down *Plin1*, we found that LD accumulation also changed significantly with changes in Plin1 expression (Figure 2). These results confirmed that Plin1 plays an important role in the accumulation of LDs in chondrocytes. Furthermore, we detected the expressions of HSL, DGAT2, and ATGL in chondrocytes induced by FGF8 and found that the expressions of DGAT2 and ATGL were not affected but that that of HSL was significantly reduced

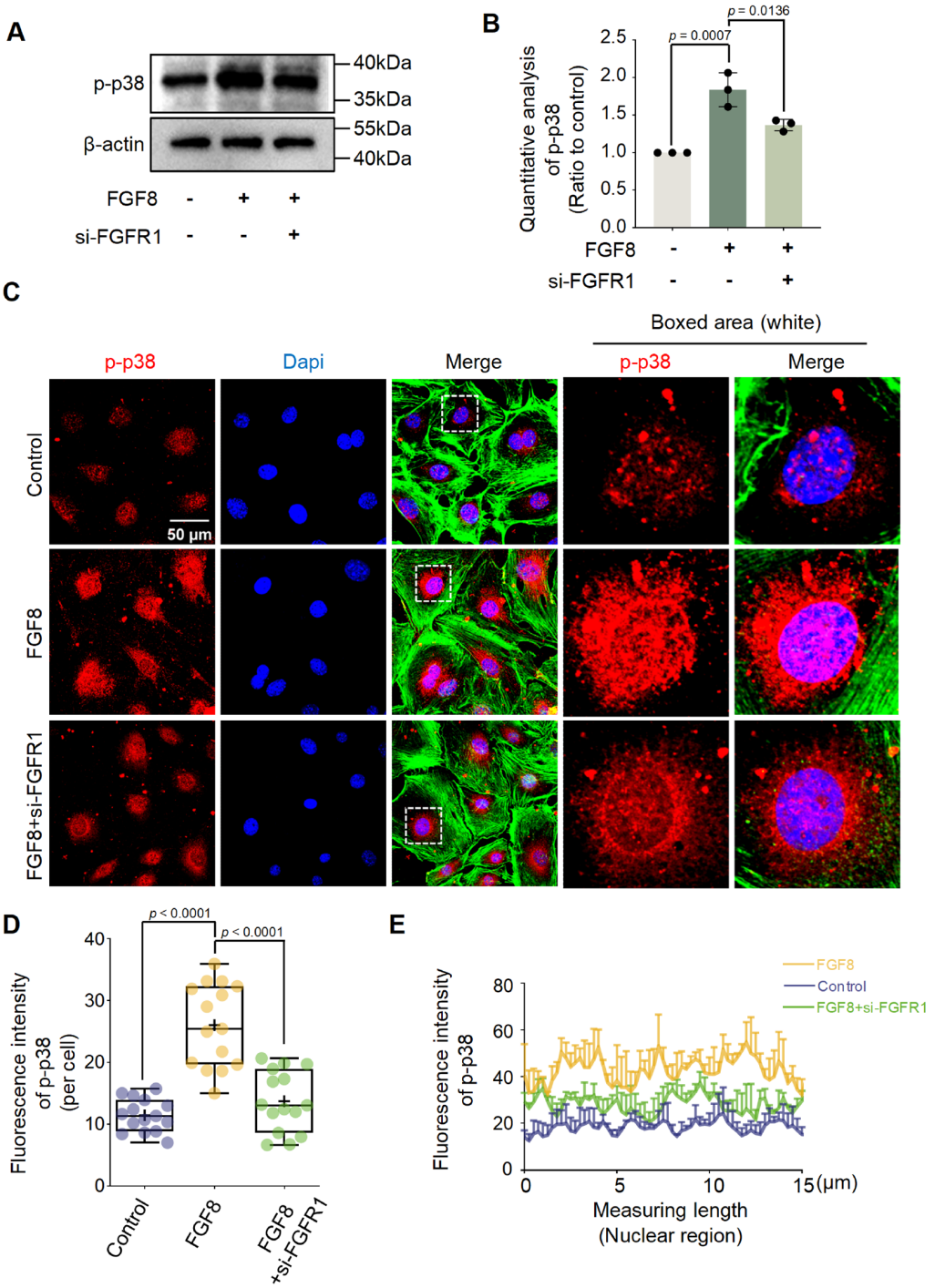

Figure 6. Knockdown of *FGFR1* downregulates p-p38 signaling (A) Western blot analysis showing the change in p-p38 signaling in chondrocytes induced by si-FGFR1 in the presence of FGF8. Chondrocytes were pretreated with siRNA for 12 h and then treated with FGF8 at 25 ng/mL for 1 h. β-Actin was used as an internal reference. (B) Quantitative analysis confirming the protein change in p-p38 in chondrocytes induced by si-FGFR1 in the presence of FGF8 at 25 ng/mL in (A). The data were based on three independent replicates ($n = 3$). (C) Representative fluorescence images showing the change in p-p38 levels in chondrocytes induced by si-FGFR1 in the presence of FGF8. Chondrocytes were pretreated with siRNA for 12 h and then treated with FGF8 at 25 ng/ml for 1 h. Images were obtained via CLSM (60×). Red fluorescence indicates p-p38, green fluorescence indicates the cytoskeleton (F-actin), and blue fluorescence indicates the nuclei. The white dashed boxes indicate the magnified regions. (D) Total fluorescence quantification per cell showing the change in p-p38 in chondrocytes induced by si-FGFR1 in the presence of FGF8 at 25 ng/mL. The data were based on 15 cells from three independent samples. (E) Representative linear fluorescence quantification of chondrocyte nuclei showing the change in nuclear accumulation of p-p38 induced by si-FGFR1 in the presence of FGF8 at 25 ng/mL. The average nuclear length was in the range of 8-15 μm. The data were based on three independent replicates ($n = 3$). The data in (B and D) were analyzed using one-way analysis of variance. The data in (B) are presented as the mean ± SD. The data in (D) are shown in box (from 25%, 50% to 75%) and whisker (minimum to maximum) plots. Differences were considered statistically significant at $P < 0.05$.

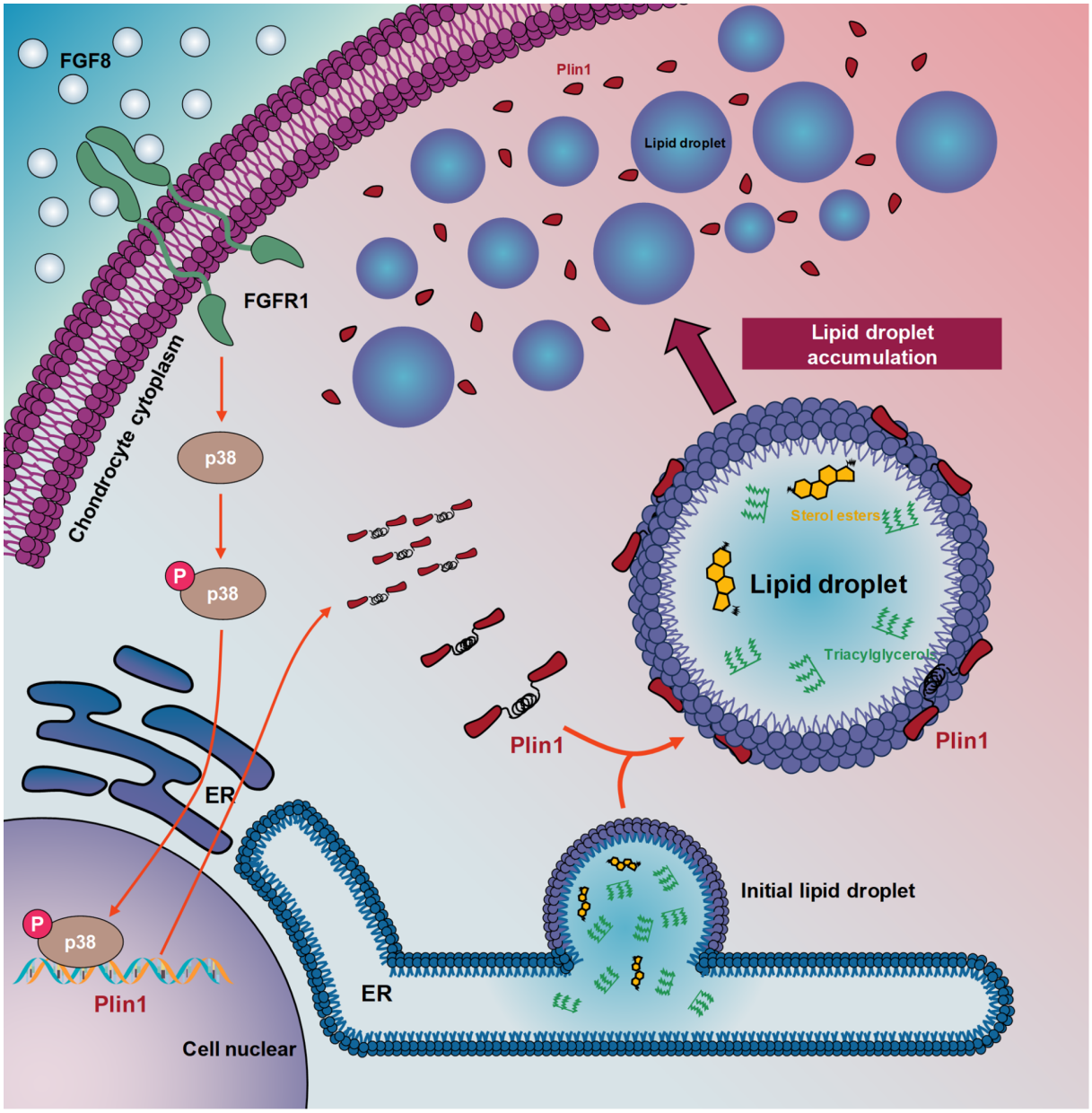

Figure 7. Schematic diagram illustrating the regulatory mechanism of lipid droplet accumulation in chondrocytes following exposure to FGF8 FGF8 binds to FGFR1 and activates p-p38 signaling in chondrocytes. Downstream signaling promotes the expression of plin1, which facilitates the encapsulation of lipid droplets and ultimately increases lipid droplet accumulation in chondrocytes.

(Supplementary Figure S4). HSL is a vital lipolytic enzyme that hydrolyzes triglycerides [69]. There is a reason to infer that their combined effect on the increase in Plin1 and decrease in HSL enhances lipid accumulation and LD formation. Notably, Plin1 is not the only factor that regulates lipid accumulation in chondrocytes, and many other factors are involved, as shown in Figure 2A and Supplementary Figure S3. For example, apolipoprotein L6 (apol6) is upregulated in chondrocytes exposed to FGF8 [68]. Previous reports have shown that apol6 can form a complex with Plin1, which prevents Plin1 from binding to HSL, thereby inhibiting lipolysis and increasing LD accumulation in adipose tissue. Taken together, these results indicate that a series of regulatory protein mediators, including Plin1, promote lipid accumulation and LD formation induced by FGF8.

FGF signals enter the cellular cytoplasm mainly via FGF receptors (FGFR1–4) [57,70]. Chondrocytes in different zones of cartilage spatiotemporally express FGFRs [71]. During cartilage development, chondrocytes highly express FGFR3 in the superficial zone and FGFR1 and 2 in the hypertrophic and calcified zones [64]. These receptors selectively recognize their FGF ligands, thereby allowing the entry of FGF signals to regulate the physiological and pathological behaviors of chondrocytes. For example, FGF2 increases the catabolic activity of human articular chondrocytes via FGFR1 [72–74]. FGF18 has been shown to facilitate chondrogenesis through FGFR3 [75]. Yellapragada *et al.* [76] reported that FGF8 binds to FGFR1 to regulate the differentiation of hypothalamic

neurons that express gonadotropin-releasing hormones. Jacques *et al.* [77] demonstrated that FGF8 binds to FGFR3 to promote cochlear development in mammals. In chondrocytes, we found that FGF8 mediates LD accumulation via FGFR1 (Figure 3 and Supplementary Figure S10). Given that FGFR1 expression is elevated in cartilage during OA progression and that its inhibition attenuates OA-associated inflammation [48,64], the potential role of FGFR1 in OA pathogenesis warrants attention because of its ability to target LD accumulation.

Previous studies have reported that FGFs relay signals to cytoplasmic MAPK, PI3K/AKT, NF-κB, or β-catenin/Wnt signaling to regulate target gene expression [44,64,78]. For example, FGF2 has been shown to mediate the elongation of primary cilia in chondrocytes, mainly through Erk signaling [79], and to modulate chondrocyte differentiation through crosstalk between Erk and β-catenin/WNT signaling [80]. FGF23 has been reported to accelerate chondrocyte hypertrophy and degeneration of the OA cartilage matrix via β-catenin/WNT signaling [81]. Lin *et al.* [82] reported that FGF8 activates PI3K/AKT and p-p38 signaling to regulate the pace of tooth development. FGF8 can also activate β-catenin/WNT signaling to induce the differentiation of dental mesenchymal cells into odontoblast-like cells [83]. We previously reported that FGF8 activates NF-κB signaling to upregulate the expression of matrix metalloproteinases 2 and 9 (MMP-2 & -9) in chondrocytes [48]. In this study, we showed that FGF8 activates MAPKs, including Erk and p38, in chondrocytes (the expression of p38 was much greater than that of Erk; Figure 4A,B) and revealed the importance of p-p38 signaling in FGF8-mediated LD accumulation via its inhibition with SB203580 (Figure 5). These findings are consistent with reports that MAPK/p38 signaling is regulated by FGF8 [56]. In addition, some reports have correlated p-p38 signaling with lipid metabolism. Liu *et al.* [84] demonstrated that the upregulation of p-p38 signaling in macrophages promotes lipid accumulation following activation by reactive oxygen species. Li *et al.* [85] reported that the upregulation of p-p38 signaling in HCT-116 cancer cells enhances lipid accumulation by promoting triacylglycerol biosynthesis [85]. In this study, we established an association between p-p38 and LD accumulation via the Plin1 protein in chondrocytes.

In conclusion, in the present study, we found that FGF8 promotes LD accumulation in chondrocytes by increasing Plin1 expression through FGFR1/p38 signaling. These findings improve our understanding of LDs in chondrocytes and provide potential therapeutic targets for cartilage diseases.

Supplementary Data

Supplementary data is available at *Acta Biochimica et Biophysica Sinica* online.

Funding

This work was supported by the grants from the National Natural Science Foundation of China (No. 81771047) and the Sichuan Science and Technology Innovation Talent Project (No. 2022JDRC0044).

Conflict of Interest

The authors declare that they have no conflict of interest.

References

1. Walther TC, Farese Jr RV. Lipid droplets and cellular lipid metabolism. *Annu Rev Biochem* 2012, 81: 687–714
2. Zadoorian A, Du X, Yang H. Lipid droplet biogenesis and functions in health and disease. *Nat Rev Endocrinol* 2023, 19: 443–459
3. Zhang C, Liu P. The lipid droplet: a conserved cellular organelle. *Protein Cell* 2017, 8: 796–800
4. Walther TC, Chung J, Farese Jr. RV. Lipid droplet biogenesis. *Annu Rev Cell Dev Biol* 2017, 33: 491–510
5. Thiam AR, Ikonen E. Lipid droplet nucleation. *Trends Cell Biol* 2021, 31: 108–118
6. Meng Y, Guo D, Lin L, Zhao H, Xu W, Luo S, Jiang X, ***et al.*** Glycolytic enzyme PFKL governs lipolysis by promoting lipid droplet-mitochondria tethering to enhance β-oxidation and tumor cell proliferation. *Nat Metab* 2024, 6: 1092–1107
7. Menon D, Bhapkar A, Manchandia B, Charak G, Rathore S, Jha RM, Nahak A, ***et al.*** ARL8B mediates lipid droplet contact and delivery to lysosomes for lipid remobilization. *Cell Rep* 2023, 42: 113203
8. Zhang S, Peng X, Yang S, Li X, Huang M, Wei S, Liu J, ***et al.*** The regulation, function, and role of lipophagy, a form of selective autophagy, in metabolic disorders. *Cell Death Dis* 2022, 13: 132
9. Lin J, Wang X, Gu M, Chen Y, Xu J, Chau NV, Li J, ***et al.*** Geniposide ameliorates atherosclerosis by restoring lipophagy via suppressing PARP1/PI3K/AKT signaling pathway. *Phytomedicine* 2024, 129: 155617
10. Olzmann JA, Carvalho P. Dynamics and functions of lipid droplets. *Nat Rev Mol Cell Biol* 2019, 20: 137–155
11. Mathiowetz AJ, Olzmann JA. Lipid droplets and cellular lipid flux. *Nat Cell Biol* 2024, 26: 331–345
12. Roberts MA, Olzmann JA. Protein quality control and lipid droplet metabolism. *Annu Rev Cell Dev Biol* 2022, 36: 115–139
13. Arlt H, Sui X, Folger B, Adams C, Chen X, Remme R, Hamprecht FA, ***et al.*** Seipin forms a flexible cage at lipid droplet formation sites. *Nat Struct Mol Biol* 2022, 29: 194–202
14. Salo VT, Belevich I, Li S, Karhinen L, Vihinen H, Vigouroux C, Magré J, ***et al.*** Seipin regulatesER –lipid droplet contacts and cargo delivery. *EMBO J* 2016, 35: 2699–2716
15. Chen C, Zhao W, Lu X, Ma Y, Zhang P, Wang Z, Cui Z, ***et al.*** AUP1 regulates lipid metabolism and induces lipid accumulation to accelerate the progression of renal clear cell carcinoma. *Cancer Sci* 2022, 113: 2600–2615
16. Klemm EJ, Spooner E, Ploegh HL. Dual role of ancient ubiquitous protein 1 (AUP1) in lipid droplet accumulation and endoplasmic reticulum (ER) protein quality control. *J Biol Chem* 2011, 286: 37602–37614
17. Malis Y, Armoza-Eilat S, Nevo-Yassaf I, Dukhovny A, Sklan EH, Hirschberg K. Rab1b facilitates lipid droplet growth by ER–to–lipid droplet targeting of DGAT2. *Sci Adv* 2024, 10: eade7753
18. Smith CE, Tsai YC, Liang YH, Khago D, Mariano J, Li J, Tarasov SG, ***et al.*** A structurally conserved site in AUP1 binds the E2 enzyme UBE2G2 and is essential for ER-associated degradation. *PLoS Biol* 2021, 19: e3001474
19. Zhang J, Zamani M, Thiele C, Taher J, Amir Alipour M, Yao Z, Adeli K. AUP1 (ancient ubiquitous protein 1) is a key determinant of hepatic very-low–density lipoprotein assembly and secretion. *Arterioscler Thromb Vasc Biol* 2017, 37: 633–642
20. Sztalryd C, Brasaemle DL. The perilipin family of lipid droplet proteins: Gatekeepers of intracellular lipolysis. *Biochim Biophys Acta (BBA)-Mol Cell Biol Lipids* 2017, 1862: 1221–1232
21. Miner GE, So CM, Edwards W, Ragusa JV, Wine JT, Wong Gutierrez D, Airola MV, ***et al.*** PLIN5 interacts with FATP4 at membrane contact sites to promote lipid droplet-to-mitochondria fatty acid transport. *Dev Cell* 2023, 58: 1250–1265.e6
22. Liu Y, Duan M, Zhang D, Xie J. The role of mechano growth factor in

chondrocytes and cartilage defects: a concise review. *Acta Biochim Biophys Sin* 2023, 55: 701–712
23. Du X, Cai L, Xie J, Zhou X. The role of TGF-beta3 in cartilage development and osteoarthritis. *Bone Res* 2023, 11: 2
24. Zhou C, Yang Y, Duan M, Chen C, Pi C, Zhang D, Liu X, ***et al.*** Biomimetic fibers based on equidistant micropillar arrays determines chondrocyte fate via mechanoadaptability. *Adv Healthcare Mater* 2023, 12: e2301685
25. Duan M, Xia S, Liu Y, Pu X, Chen Y, Zhou Y, Huang M, ***et al.*** Stiffened fibre-like microenvironment based on patterned equidistant micropillars directs chondrocyte hypertrophy. *Mater Today Bio* 2023, 20: 100682
26. Xie J, Zhang D, Lin Y, Yuan Q, Zhou X. Anterior cruciate ligament transection–induced cellular and extracellular events in menisci: implications for osteoarthritis. *Am J Sports Med* 2018, 46: 1185–1198
27. Zhuo Q, Yang W, Chen J, Wang Y. Metabolic syndrome meets osteoarthritis. *Nat Rev Rheumatol* 2012, 8: 729–737
28. Seow SR, Mat S, Ahmad Azam A, Rajab NF, Safinar Ismail I, Singh DKA, Shahar S, ***et al.*** Impact of diabetes mellitus on osteoarthritis: a scoping review on biomarkers. *Expert Rev Mol Med* 2024, 26: e8
29. Peiris CL, Culvenor AG. Metabolic syndrome and osteoarthritis: implications for the management of an increasingly common phenotype. *Osteoarthritis Cartilage* 2023, 31: 1415–1417
30. Park S, Baek IJ, Ryu JH, Chun CH, Jin EJ. PPARα-ACOT12 axis is responsible for maintaining cartilage homeostasis through modulating de novo lipogenesis. *Nat Commun* 2022, 13: 3
31. Wang H, Shi Y, He F, Ye T, Yu S, Miao H, Liu Q, ***et al.*** GDF11 inhibits abnormal adipogenesis of condylar chondrocytes in temporomandibular joint osteoarthritis. *Bone Joint Res* 2022, 11: 453–464
32. Zhang X, Pu X, Pi C, Xie J. The role of fibroblast growth factor 7 in cartilage development and diseases. *Life Sci* 2023, 326: 121804
33. Kan S, Duan M, Liu Y, Wang C, Xie J. Role of mitochondria in physiology of chondrocytes and diseases of osteoarthritis and rheumatoid arthritis. *Cartilage* 2021, 13: 1102S–1121S
34. Yang Y, Wei J, Li J, Cui Y, Zhou X, Xie J. Lipid metabolism in cartilage and its diseases: a concise review of the research progress. *Acta Biochim Biophys Sin* 2021, 53: 517–527
35. Su Z, Zong Z, Deng J, Huang J, Liu G, Wei B, Cui L, ***et al.*** Lipid metabolism in cartilage development, degeneration, and regeneration. *Nutrients* 2022, 14: 3984
36. Lippiello L, Walsh T, Fienhold M. The association of lipid abnormalities with tissue pathology in human osteoarthritic articular cartilage. *Metabolism* 1991, 40: 571–576
37. Gkretsi V, Simopoulou T, Tsezou A. Lipid metabolism and osteoarthritis: Lessons from atherosclerosis. *Prog Lipid Res* 2011, 50: 133–140
38. Goldring MB, Berenbaum F. The regulation of chondrocyte function by proinflammatory mediators. *Clin Orthopaedics Relat Res* 2004, 427: S37–S46
39. Haeggström JZ, Funk CD. Lipoxygenase and leukotriene pathways: biochemistry, biology, and roles in disease. *Chem Rev* 2011, 111: 5866–5898
40. Schmidt S, Klampfleuthner FAM, Renkawitz T, Diederichs S. Cause and chondroprotective effects of prostaglandin E2 secretion during mesenchymal stromal cell chondrogenesis. *Eur J Cell Biol* 2024, 103: 151412
41. Wu X, Sun ARJ, Crawford R, Xiao Y, Wang Y, Prasadam I, Mao X. Inhibition of leukotriene A_4 hydrolase suppressed cartilage degradation and synovial inflammation in a mouse model of experimental osteoarthritis. *Cartilage* 2024, 15: 184–194
42. Corbet C, Bastien E, Santiago de Jesus JP, Dierge E, Martherus R, Vander Linden C, Doix B, ***et al.*** TGFβ2-induced formation of lipid droplets supports acidosis-driven EMT and the metastatic spreading of cancer cells. *Nat Commun* 2020, 11: 454
43. Matsuzawa T, Morita M, Shimane A, Otsuka R, Mei Y, Irie F, Yamaguchi Y, ***et al.*** Heparan sulfate promotes differentiation of white adipocytes to maintain insulin sensitivity and glucose homeostasis. *J Biol Chem* 2021, 297: 101006
44. Chen H, Cui Y, Zhang D, Xie J, Zhou X. The role of fibroblast growth factor 8 in cartilage development and disease. *J Cell Mol Medi* 2022, 26: 990–999
45. Maddaluno L, Urwyler C, Werner S. Fibroblast growth factors: key players in regeneration and tissue repair. *Development* 2017, 144: 4047–4060
46. Liu H, Fang Q, Wang M, Wang W, Zhang M, Zhang D, He Y, ***et al.*** FGF8 and FGFR3 are up-regulated in hypertrophic chondrocytes: association with chondrocyte death in deep zone of Kashin-Beck disease. *Biochem Biophys Res Commun* 2018, 500: 184–190
47. Uchii M, Tamura T, Suda T, Kakuni M, Tanaka A, Miki I. Role of fibroblast growth factor 8 (FGF8) in animal models of osteoarthritis. *Arthritis Res Ther* 2008, 10: R90
48. Huang H, Xie J, Wei J, Xu S, Zhang D, Zhou X. Fibroblast growth factor 8 (FGF8) up-regulates gelatinase expression in chondrocytes through nuclear factor-κB p65. *J Bone Miner Metab* 2023, 41: 17–28
49. Duan M, Liu Y, Pi C, Zhao Y, Tian Y, Xie J. TGF-β2 enhances nanoscale cortex stiffness via condensation of cytoskeleton-focal adhesion plaque. *Biophys J* 2025, 124: 336–350
50. Zhou C, Cui Y, Yang Y, Guo D, Zhang D, Fan Y, Li X, ***et al.*** Runx1 protects against the pathological progression of osteoarthritis. *Bone Res* 2021, 9: 50
51. Liu Y, Pu X, Duan M, Chen C, Zhao Y, Zhang D, Xie J. Biomimetic fibers derived from an equidistant micropillar platform dictate osteocyte fate via mechanoreception. *Nano Lett* 2023, 23: 7950–7960
52. Zhang L, Duan M, Pu X, Zheng H, Ning X, Tu Y, Xu C, ***et al.*** GroEL triggers NLRP3 inflammasome activation through the TLR/NF-kappaB p-p65 axis in human periodontal ligament stem cells. *Acta Biochim Biophys Sin* 2024, 56: 1340–1351
53. Zhang L, Zhang D, Liu C, Tang B, Cui Y, Guo D, Duan M, ***et al.*** Outer membrane vesicles derived from *fusobacterium nucleatum* trigger periodontitis through host overimmunity. *Adv Sci* 2024, 11: e2400882
54. Abshirini M, Ilesanmi-Oyelere BL, Kruger MC. Potential modulatory mechanisms of action by long-chain polyunsaturated fatty acids on bone cell and chondrocyte metabolism. *Prog Lipid Res* 2021, 83: 101113
55. Bozza PT, Viola JP. Lipid droplets in inflammation and cancer. *Prostaglandins Leukot Essent Fatty Acids* 2010, 82: 243–250
56. Cao X, Cai L, Guo D, Zhang D, Zhou X, Xie J. Fibroblast growth factor 8 facilitates cell-cell communication in chondrocytes via p38-MAPK signaling. *Tissue Cell* 2023, 83: 102155
57. Ellman MB, Yan D, Ahmadinia K, Chen D, An HS, Im HJ. Fibroblast growth factor control of cartilage homeostasis. *J Cell Biochem* 2013, 114: 735–742
58. Chen W, Wang Q, Tao H, Lu L, Zhou J, Wang Q, Huang W, ***et al.*** Subchondral osteoclasts and osteoarthritis: new insights and potential therapeutic avenues. *Acta Biochim Biophys Sin* 2024, 56: 499–512
59. Luria A, Chu CR. Articular cartilage changes in maturing athletes. *Sports Health* 2014, 6: 18–30
60. Bhattaram P, Chandrasekharan U. The joint synovium: a critical determinant of articular cartilage fate in inflammatory joint diseases. *Semin Cell Dev Biol* 2017, 62: 86–93
61. Huang H, Duan M, Wei J, Liu Y, Xu S, Huang M, Tu Y, ***et al.*** Fibroblast growth factor 8 (FGF8) induces mitochondrial remodeling in chondrocytes viaERK /AMPK signaling pathway. *FASEB J* 2025, 39: e70501
62. Wei J, Yang Y, Guo D, Xu S, Huang H, Zhang D, Xie J, ***et al.*** Osteoblasts induce glucose-derived ATP perturbations in chondrocytes through

noncontact communication. *Acta Biochim Biophys Sin* 2022, 54: 625–636
63. Krishnan Y, Grodzinsky AJ. Cartilage diseases. *Matrix Biol* 2018, 71-72: 51–69
64. Xie Y, Zinkle A, Chen L, Mohammadi M. Fibroblast growth factor signalling in osteoarthritis and cartilage repair. *Nat Rev Rheumatol* 2020, 16: 547–564
65. Xu J, Huang Z, Wang W, Tan X, Li H, Zhang Y, Tian W, ***et al.*** FGF8 signaling alters the osteogenic cell fate in the hard palate. *J Dent Res* 2018, 97: 589–596
66. Wei X, Li L, Zhao J, Huo Y, Hu X, Lu J, Pi J, ***et al.*** BAP31 depletion inhibited adipogenesis, repressed lipolysis and promoted lipid droplets abnormal growth via attenuating perilipin1 proteasomal degradation. *Int J Biol Sci* 2023, 19: 1713–1730
67. Sun Z, Gong J, Wu H, Xu W, Wu L, Xu D, Gao J, ***et al.*** Perilipin1 promotes unilocular lipid droplet formation through the activation of Fsp27 in adipocytes. *Nat Commun* 2013, 4: 1594
68. Wang Y, Nguyen HP, Xue P, Xie Y, Yi D, Lin F, Dinh J, ***et al.*** ApoL6 associates with lipid droplets and disrupts Perilipin1-HSL interaction to inhibit lipolysis. *Nat Commun* 2024, 15: 186
69. Birnbaum MJ. Lipolysis. *J Cell Biol* 2003, 161: 1011–1012
70. Cinque L, Forrester A, Bartolomeo R, Svelto M, Venditti R, Montefusco S, Polishchuk E, ***et al.*** FGF signalling regulates bone growth through autophagy. *Nature* 2015, 528: 272–275
71. Miraoui H, Marie PJ. Fibroblast growth factor receptor signaling crosstalk in skeletogenesis. *Sci Signal* 2010, 3: re9
72. Yan D, Chen D, Cool SM, van Wijnen AJ, Mikecz K, Murphy G, Im HJ. Fibroblast growth factor receptor 1 is principally responsible for fibroblast growth factor 2-induced catabolic activities in human articular chondrocytes. *Arthritis Res Ther* 2011, 13: R130
73. Liu Z, Xu J, Colvin JS, Ornitz DM. Coordination of chondrogenesis and osteogenesis by fibroblast growth factor 18. *Genes Dev* 2002, 16: 859–869
74. Wang Q, Green RP, Zhao G, Ornitz DM. Differential regulation of endochondral bone growth and joint development by FGFR1 and FGFR3 tyrosine kinase domains. *Development* 2001, 128: 3867–3876
75. Davidson D, Blanc A, Filion D, Wang H, Plut P, Pfeffer G, Buschmann MD, ***et al.*** Fibroblast growth factor (FGF) 18 signals through FGF receptor 3 to promote chondrogenesis. *J Biol Chem* 2005, 280: 20509–20515
76. Yellapragada V, Eskici N, Wang Y, Madhusudan S, Vaaralahti K, Tuuri T, Raivio T. FGF8-FGFR1 signaling regulates human GnRH neuron differentiation in a time- and dose-dependent manner. *Dis Model Mech* 2022, 15: dmm049436
77. Jacques BE, Montcouquiol ME, Layman EM, Lewandoski M, Kelley MW. Fgf8 induces pillar cell fate and regulates cellular patterning in the mammalian cochlea. *Development* 2007, 134: 3021–3029
78. Cao X, Cui Z, Ding Z, Chen Y, Wu S, Wang X, Huang J. An osteoarthritis subtype characterized by synovial lipid metabolism disorder and fibroblast-like synoviocyte dysfunction. *J Orthopaedic Translation* 2022, 33: 142–152
79. Kunova Bosakova M, Varecha M, Hampl M, Duran I, Nita A, Buchtova M, Dosedelova H, ***et al.*** Regulation of ciliary function by fibroblast growth factor signaling identifies FGFR3-related disorders achondroplasia and thanatophoric dysplasia as ciliopathies. *Hum Mol Genet* 2018, 27: 1093–1105
80. Buchtova M, Oralova V, Aklian A, Masek J, Vesela I, Ouyang Z, Obadalova T, ***et al.*** Fibroblast growth factor and canonical WNT/β-catenin signaling cooperate in suppression of chondrocyte differentiation in experimental models of FGFR signaling in cartilage. *Biochim Biophys Acta Mol Basis Dis* 2015, 1852: 839–850
81. Meo Burt P, Xiao L, Hurley MM. FGF23 regulates Wnt/β-catenin signaling-mediated osteoarthritis in mice overexpressing high-molecular-weight FGF2. *Endocrinology* 2018, 159: 2386–2396
82. Lin C, Ruan N, Li L, Chen Y, Hu X, Chen YP, Hu X, ***et al.*** FGF8-mediated signaling regulates tooth developmental pace during odontogenesis. *J Genet Genomics* 2022, 49: 40–53
83. Kimura M, Saito A, Onodera S, Nakamura T, Suematsu M, Shintani S, Azuma T. The concurrent stimulation of Wnt and FGF8 signaling induce differentiation of dental mesenchymal cells into odontoblast-like cells. *Med Mol Morphol* 2022, 55: 8–19
84. Liu J, Wei Y, Jia W, Can C, Wang R, Yang X, Gu C, ***et al.*** Chenodeoxycholic acid suppresses AML progression through promoting lipid peroxidation via ROS/p38 MAPK/DGAT1 pathway and inhibiting M2 macrophage polarization. *Redox Biol* 2022, 56: 102452
85. Li N, Saitou M, Atilla-Gokcumen GE. The role of p38 MAPK in triacylglycerol accumulation during apoptosis. *Proteomics* 2019, 19: e1900160